Far-Infrared Cyclotron Resonance in Cadmium Sulfide

Giyuu Kido

Department of Material Physics
Engineering Science
Osaka University

March 1973

ABSTRACT

A technique has been developed for the purpose of observing far-infrared cyclotron resonance in compound semiconductors having relatively heavy mass and low mobility of carriers at high temperature. In the apparatus a Cu-2%Be helical solenoid is used for a pulsed magnet which is available up to 350 kOe and as the light source, an H_2O laser (119 μm) and an HCN laser (337 μm) are used in pulsed operation. Moreover, by employing a new designed cryostat, the temperature of the specimen in the field can be varied from 4.2 K to 250 K.

The far-infrared cyclotron resonance measurements in CdS have been carried out by means of the above technique in the temperature range from 25 K to 250 K. The electron cyclotron mass in CdS increases with temperature up to 50 K and shows a constant value above 50 K. Besides, in the far-infrared cyclotron resonance spectra a sub-band appears at about 85 kOe. The sub-band is attributed to the optical phonon of the wave number 43 cm^{-1} which was discovered recently in the Raman spectra by Porto et al.

The electrons in CdS are considered to be piezoelectric polarons, so that the cyclotron mass of the electrons may show temperature dependence. The present experimental results agree qualitatively with the results of theoretical calculations for the piezoelectric polarons as long as the temperature dependence of the resonance line width in the spectra and the magnetic field dependence of the cyclotron mass are concnerned. However, there is a contradiction between the experimental results of temperature dependence of the cyclotron mass shift and the theories. An advanced theory is required for the sufficient explanation of the present experimental results.

Acknowledgements

The author would like to express his sincere thanks to Professor S. Narita for his constant guidance and encouragement. Thanks are also due to Dr. K. Nagasaka for his helpful suggestions. Thanks are extended to the members of the laboratory of Prof. Narita for their useful discussions.

CONTENTS

1. INTRODUCTION

Cadmium sulfide crystal is a representative ionic crystal of wurtzite structure. The wurtzite structure may be considered as four interpenetrating hexagonal Bravais lattices, or equivalently as two interpenetrating hexagonal-close-packed lattices. The space group of the wurtzite structure is C_{6v}^4, $P6_{3mc}$. In the crystal, acoustic phonons give rise to macroscopic stress waves. Then, the acoustic phonons are belived to interact with electrons in cadmium sulfide through the longitudinal piezoelectric field wave.

Meijer and Polder[1] theoretically studied electron mobilities in piezoelectric materials in all temperature range, taking the interaction between an electron and acoustic phonons and that between an electron and optical phonons into consideration. They predicted conclusively that in zinc-sulfide crystal of the sphalerite structure the electron mobility is mainly determined by the acoustic phonon scattering in the temperature range below 100 K and by the optical phonon scattering in the temperature range above 120 K. Piper and Halsted[2] made the measurements of the mobility in cadmium sulfide in the temperature region from 15 K to 700 K using the standard d.c. technique. However, they could not observe the temperature dependence of the mobility due to the piezoelectric scattering even in the low temperature region. Moreover, Fujita et al.[3] carried out the experiment of Photo-Hall effects of photo-excited electrons in cadmium sulfide crystal by means of Kobayashi-Brown methods[4]. They concluded that the acoustic phonon scattering is dominant for the mobility below 25 K, while the optical phonon scattering dominant for the mobility above 100 K.

In the electron-phonon interaction in cadmium sulfide, it is more interesting to study the polaron-mass shifts than the scattering,

from the reasons mentioned below. By measuring the magneto-optics[5] and plasma reflection[6], the effective mass was determined to be 0.2 m_o at 77 K, where m_o is the static electronic mass in vacuum. On the other hand, in the observation of the cyclotron resonance in the microwave region, Sawamoto[7] determined the effective mass to be 0.17 m_o ($c \perp H$) at 1.7 K, and Bear and Dexter[8] also determined that to be 0.162 m_o ($c \perp H$) and 0.171 m_o ($c \parallel H$) at 1.3 K, where c is the c-axis of the crystal and H is the magnetic field. Mahan and Hopfield[9] introduced the piezoelectric polaron effects in order to interpret the discrepancy between the values of the effective mass. They considered that their theory succeeded in explaining the temperature depedence of the effective mass. The theory described that the effective mass decreases with lowering temperature and is always smaller than the bare band mass. Since then, the further studies were made theoretically and experimentally on the piezoelectric polrons in the intense magnetic field ($\hbar\omega_c >> k_B T$, where k_B is the Boltzmann constant, T is the temperature and $\hbar\omega_c$ is the cyclotron resonance energy).

Larsen[10] made attempts to deal with the piezoelectric polarons in a magnetic field at the zero temperature. Saitoh and Kawabata[11] carried out calculations of the conductivity of the piezoelectric polarons in a magnetic field, by means of Kubo formula[12]. They calculated the shift of the resonant field and the change of the line width in the cyclotron resonance of the piezoelectric polarons in wide temperature range. Miyake[13] also theoretically obtained the shift and the line width in the cyclotron resonance of the piezoelectric polarons in the quantum limit ($\hbar\omega_c >> k_B T$) by calculating the shift of the energy separation between the first and the second Landau levels. The shifts of the resonant field agree in sign among these theories. However, S-K theory and M-theory show contradictory aspects in the temperature dependence of the piezoelectric polaron mass against M-H theory: the piezoelectric polaron mass decreases with temperature in S-K theory and

M-theory

Experimentally, Button et al.[14] have measured the far-infrared cyclotron resonance of electrons in cadmium sulfide using an HCN laser (337 μm) or DCN laser (195 μm) and a water cooled intense static magnet up to 230 kOe at the temperature range from 8 K to 100 K. They observed splittings of the resonance line at high temperature. Their results were not reproducible[15]. Independently the author [16),17)] has studied the far-infrared cycrotron resonance of electrons in cadmium sulfide using an H_2O laser (119μm) and a high field magnet of pulsed operation up to 350 kOe. However, we found some errors in the higher temperature spectra, caused by the miss selection of the specimen thickness and the spectral analyzer.

By developing a boxcar integrators[18] with long holding time and by using the specimen thickness matched with the carrier concentration at the measuring temperature, the author obtained reproducible experimental spectra of the far-infrared cyclotron resonance. In this paper, the experimental apparatus and the temperature dependence of the piezoelectric polarons will be reported.

In chapter 2, the experimental arrangements will be described. In chapter 3, the experimental results of far-infrared cyclotron resonance will be exhibited. In chapter 4, the author will compare the experimental results with the theory of the piezoelectric polarons developed by Miyake. And in chapter 5, we will discuss about the sub-band in the cyclotron resonance spectrum and further about the electron-phonon interactions.

2. EXPERIMENTAL PROCEDURE

2.1. Introduction

The development of various far-infrared measurements proceeded greatly in recent years with the popularization of far-infrared molecular gas lasers. In the present experiment of the cyclotron resonance, two types of lasers are used being operated at a wave length 119 μm (H_2O gas laser) and 337 μm (HCN gas laser) in a strong magnetic field.

The cyclotron resonance spectroscopy has contributed to the establishments of band-structures of many semiconductors and to the studies of scattering mechanisms in the semiconductors. Nowadays, as the frequency used in a cyclotron resonance measurement has been expanded from the microwave region to the far infrared region, the cyclotron resonance condition ($\omega_c\tau > 1$, where ω_c is the angular resonance frequency, τ, the time between collisions) has become to be easily obtained. The relaxation times are usually very large in most of compound semiconductors and even in elemental semiconductors (Ge, Si) except for low temperature ($<<30$ K). Therefore, the development of far-infrared cyclotron resonance spectrometer has been required.

On the other hand, it is natural from the relation, $\omega_c = eH/m^*c$, that the higher the used frequency become, the stronger the magnetic field must be, for the same effective mass m^*. Therefore, the utilization of the resonance spectrometer in far-infrared region requires at the same time the development of an intense magnetic field.

A pulsed electromagnet is a conventional way to obtain an intense magnetic field. The measurement in such a field, however, should be finished within a very short interval. Even in the case of pulsed magnet,

utilization of a CW laser might certainly be more preferable on account of the simplicity of the measuring cirsuit. However, the light intensity from a CW laser is frequently too weak compared with that from a pulsed laser to carry out the cyclotron resonance measurement with the materials from which we can obtain only very small signals. Moreover, it is rather appropriate to use transient light sources for picking up the phenomena just at the maximum magnetic field.

Accordingly, the pulsed laser is utilized with the pulsed magnet in our cyclotron resonance spectrometer.

2.2. General descriptions

In this section, first we will show the block diagram of the whole apparatuses in Fig. 1 to describe the behaviors of each parts. The production of the pulsed magnetic field is obtained by discharging the energy stored in condenser bank to an air-cored magnet coil. At this time, the maximum magnetic field is directly proportional to the voltage of the charged condenser, and hereafter, we denote the maximum field as the magnetic field simply. In order to generate a constant magnetic field repeatedly, the condenser is always discharged after the charged voltage is raised up just to a fixed voltage. The divided voltage of the fixed voltage is used to the X-component of X-Y recorder for representing the magnetic field. After 1.0 sec. from the completion of the condenser charging, a trigger voltage is applied to the cirsuit of the time interval ajuster from the circuit of the power supply for magnet, and the ajuster immediately instructs the power supply to discharge for the magnet, and after a while, the adjuster orders the circuit of the power supply for laser to discharge for the laser emission during the maximum field interval.

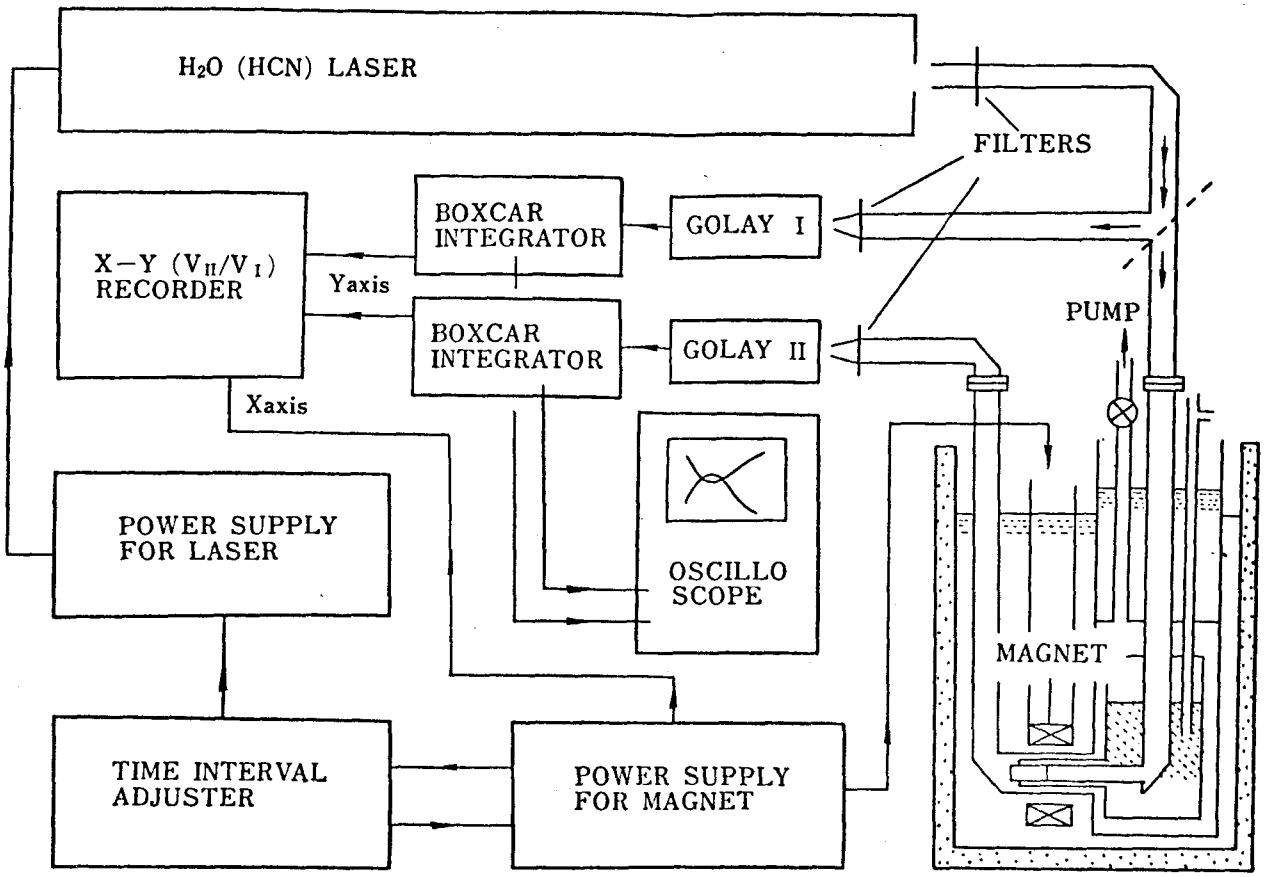

Fig. 1. Block diagram of the whole experimental arrangement for the far-infrared cyclotron resonance measurement utilizing a laser.

The laser output is guided by light pipes and after being transmitted through filters, splitted into dual beams by a beam-splitter which is made of a polyethylene plate or a qualtz plate. In the present spectroscopy, a double beam method is indispensable, because the intensity of radiation from the far-infrared laser of pulsed operation changes from one pulse to another. One beam from the splitter is introduced into a Golay cell I directly as a reference signal. The other beam, after being transmitted through the specimen under the magnetic field, is introduced into a Golay cell II.

The transmittance of the sample can be obtained as an output ratio of the Golay cells, I to II. Each output voltage of the Golay cells is storaged in a boxcar integrator and the sum of about 15 signals is transmitted into the input of the Y-component of an X-Y recorder, which operates as a divider. That is, the sum of the signals from the specimen is divided by that of the reference and ratio is recorded as the Y-component.

A detailed explanation for the operation of the electronics-system is as follows: In the first step, a condenser bank for the power supply of the magnet is charged as shown in Fig. 2A. The charging is finished when the voltage reaches a certain voltage E_0. Meanwhile the infrared laser repeats its discharge at a certain interval (1 H_z) and redischarges at the end of the condenser-charging (t_1 Fig. 2C). After a certain interval (1 sec) the condenser for magnet discharges (t_2 Fig. 2A) and after a certain interval the laser discharges according to a time schedule that the maximum magnetic field coincides with the laser emitting (t_3 Fig. 2B and 2C). The signal from the Golay cells is indicated in Fig. 2D. The integration of the signal is limitted between t_4 and t_5 (Fig. 2E)

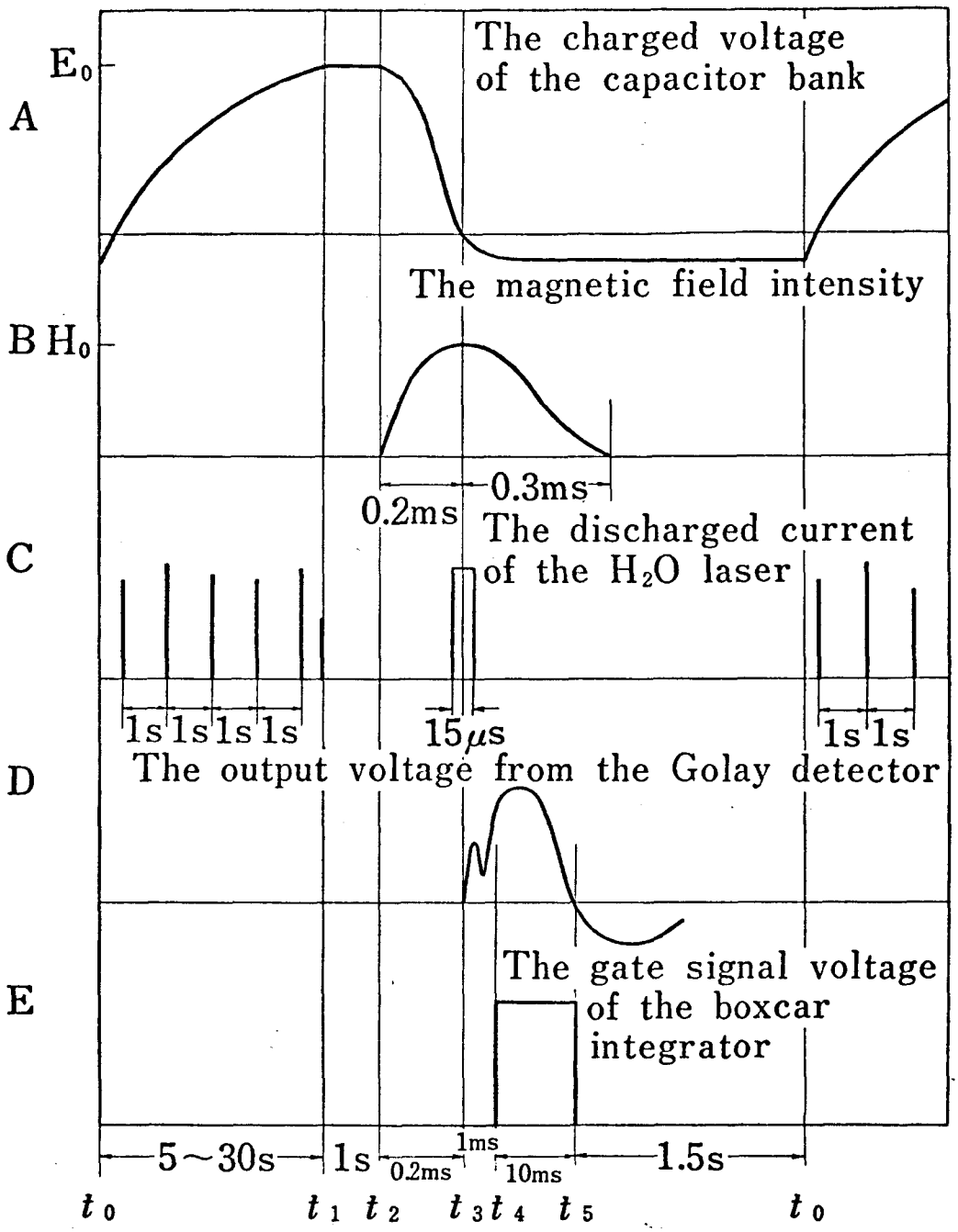

Fig. 2. The wave-forms of the voltages or field at various parts of the apparatuses are schematically shown as functions of the operating time;

A: the cahrged voltage of the condenser C(1500 μF), B: the magnetic field intensity, C: the discharged currents of the far-infrared laser, D: the output voltage from the Golay cell, E: the gate signal voltage.

for avoiding the effect from a strong electric induction due to the laser discharge and the strong magnetic field.

2.3. Detailed Descriptions

2.3.1. Far-infrared lasers

Fig. 3 shows a schematic diagram of an H_2O (or HCN) laser used in this experiment. The dimension of the H_2O laser is 2400mm in length and that of the HCN laser is 4000mm, the inner diameter is 95^{ϕ} and the coupling hole 10^{ϕ}, respectively. For the H_2O laser the inner gas pressure is 0.4 $\sim$ 0.8 torr, and for the HCN laser 0.5 $\sim$ 0.8 torr mixed CH_4 + N_2 gas was used. Generally, gas lasers in pulsed operation draw non-equal time-intervals between the voltage application and the discharge from one pulse to another. This irregular delay time makes the settlement of the time schedule very difficult. In other words, the laser emission not always coincides with the maximum magnetic field in this case. In order to eliminate this difficulty, the gas in the laser tube is ceaselessly ionized in part by using a tesla-coil, in this way the gas is ready to discharge. By this method, the time-intervals became negligibly small.

There are many lines in H_2O laser output, 23, 47, 79, 119 and 220 micron lines. Yoshinaga filters are used to eliminate higher frequency lines than 119 μm, and $^{\#}150$ mesh filters are used as the band-pass filter.

The HCN laser emits 337 μm line mainly, and the other line (311 μm) is weaker by an order and can be removed, if necessary, by tuning with a movable mirror. For the elimination of the visible light, we employed black polyethylene filters.

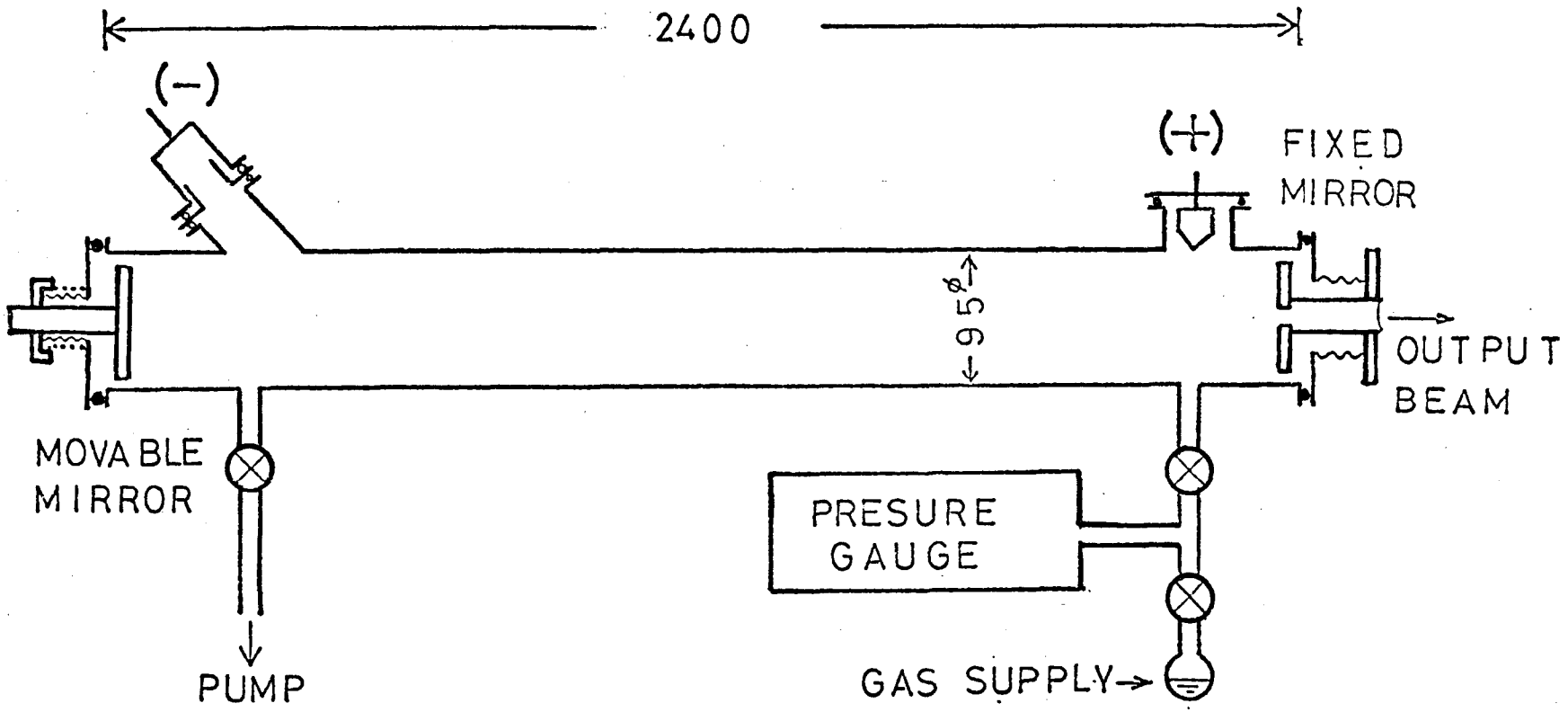

Fig. 3. Far-infrared laser used as the light source in cyclotron resonance measurement.

2.3.2 Cryostat and high field magnet

The conditions required for the present experiment are the magnetic field intensities as large as 350 kOe in addition to the specimen temperature range from liquid helium to 250 K. The magnet and the cryostat are used being immersed in a liquid nitrogen bath directly. The main difficulty is that the temperature of the specimen confined within a narrow space must be changed for a wide range with accuracy, while the small I.D. of the magnet is required to strengthen the field. As shown in Fig. 4, the part of the apparatus submerged under the liquid nitrogen bath can be divided into a cryostat part and a magnet part. Far-infrared light beam is introduced through a light pipe system onto the specimen and goes out through another light pipe system after going through a window.

Attentions are particularly paid for the mechanism on

(1) easy replacement of specimen,

(2) accurate temperature control and measurement, and

(3) easy removal and resetting of the component-pieces.

i) Vacuum sealing at low temperature

Requirements for the above mentioned (1) and (3), a special divice of sealing should be necessary for each joint with screw, except for soldered parts. Generally, indium-O-rings are conventionally employed for low temperature sealings. However, the method alone does not make a useful sealing in the present case, because the strong impact due to the pulsed magnet often breaks the vacuum-sealings. Avoiding this difficulty, we utilized brass screws and iron washers together with indium-O-rings. The reason is that the difference in the thermal expansion coefficients for indium, brass and iron works effectively for making the sealing tight

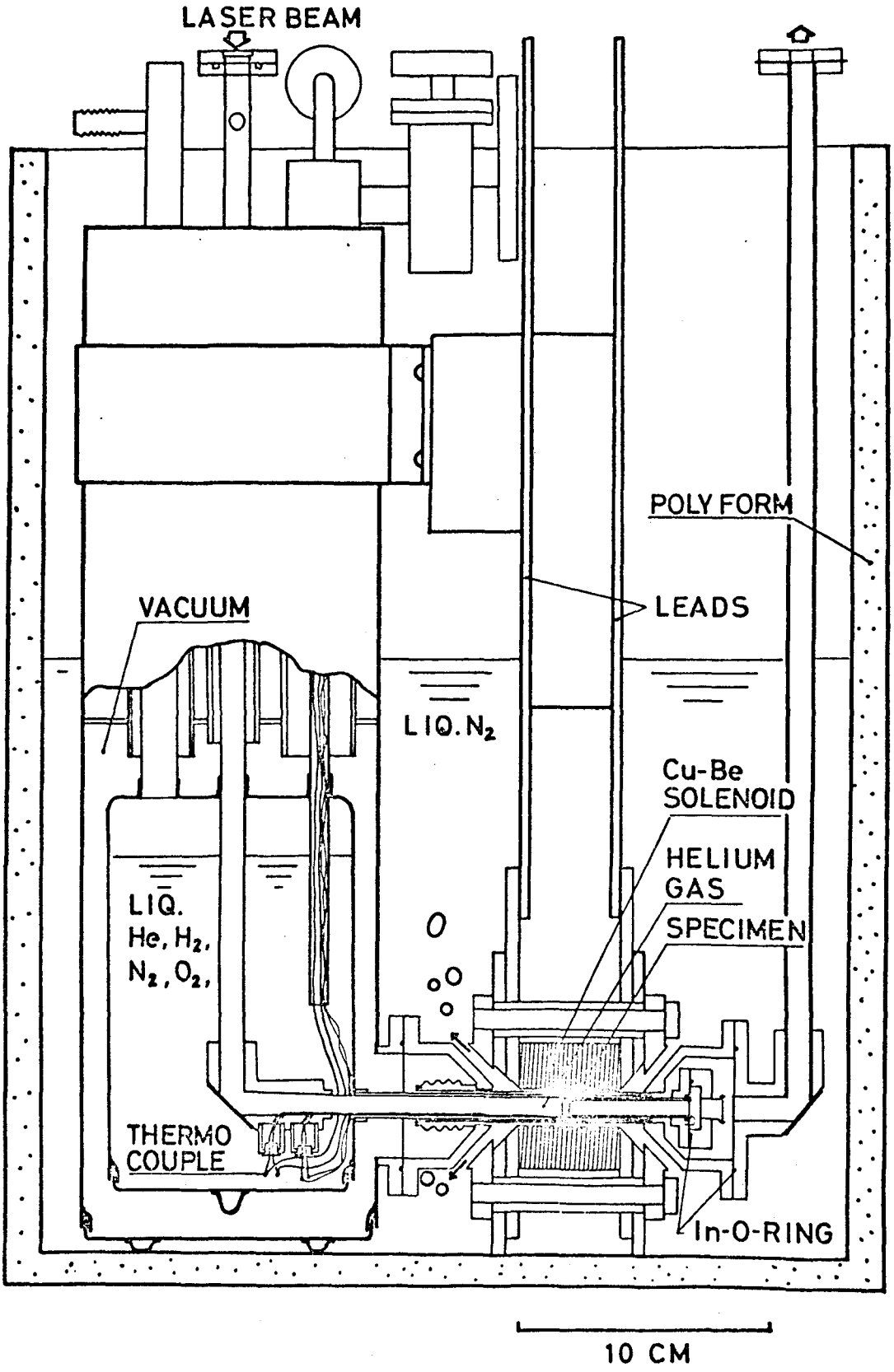

Fig. 4. Cryostat and the magnet.

during temperature-lowering.

ii) Temperature control of the specimen

It was required for us to introduce coolants arround the specimen for cooling it down acculately, therefore the threefold stainless-steel pipes are used, the structures of which are shown fully in Fig. 5. The space between the pipes 12^{ϕ} and 10^{ϕ} is evacuated to keep the inner pipe from thermal contact with the outer liquid nitrogen. The coolant liquid can circulate in the space between the pipes 10^{ϕ} and 8^{ϕ}. In order to expanding the possible temperature range for the experiment, a heater was wound around the specimen and we could change the specimen temperature by the heater and by selecting the coolant among liq. He, liq. H_2, liq.N_2 and liq. O_2. The temperature of the specimen is known by a thermo-couple set (Au(Co)-Chromel p or Constantan-Chromel p) as the temperature difference of the specimen room from the coolant. The specimen holder is composed of twofold pipes having a longitudinal slit to avoid induction currents by the intense transient magnetic field, and the specimen is set in an almost closed room made of two polyethylene plates and the twofold pipes. We regard the temperature of the specimen as being almost equal to the temperature of the inner pipe at which the thermo-couple set is soldered.

Fig. 6 shows a temperature control circuit used for checking and fixing the temperature of the specimen accurately. The output of an amplified vlotage of the thermo-couple set is compared with a certain voltage corresponding to the fixed temperature in a differential amplifier. The output of the differential amplifier controls the power supply for heater through the hyblid p.i.d. circuit which is adjusted as minimizing

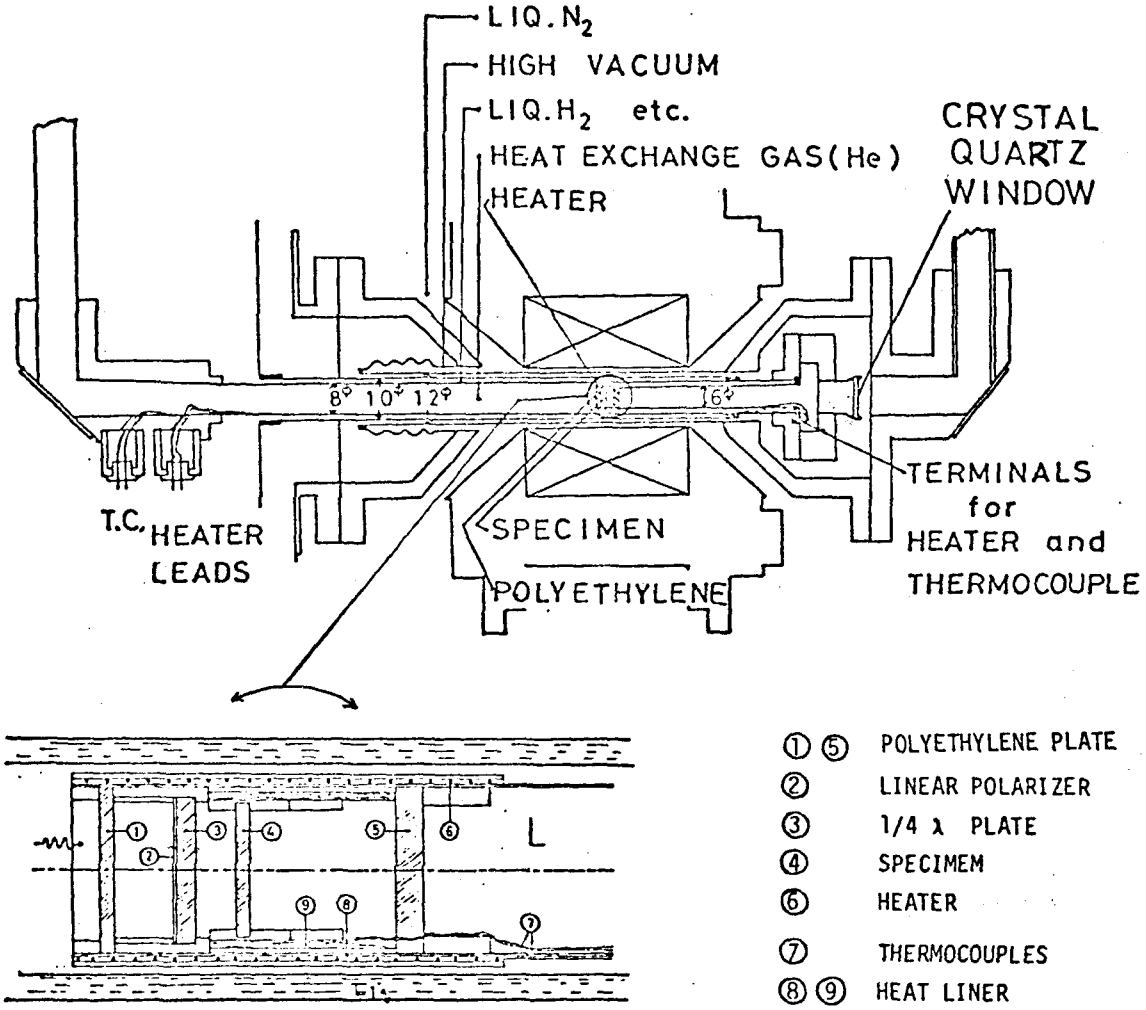

Fig. 5. Details of the cryostat.

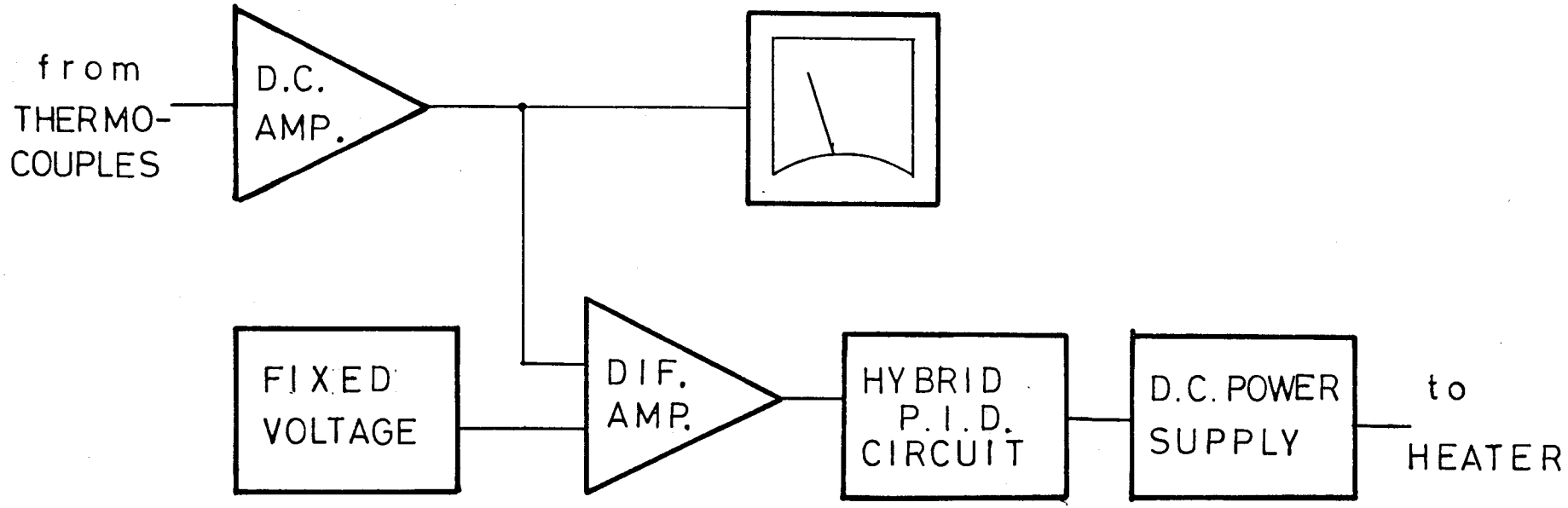

Fig. 6. Block diagram of the temperature control circuit.

the temperature fluctuation.

On the other hand, as the temperature of the threefold pipes are easily heated up by magnetic induction, the temperature of specimen is raised by the heat-radiation and the thermal conduction. However, the temperature of the specimen is considered unchanged from the settled temperature during the short interval about 200 micro-seconds of the transient field, therefore, the temperature-rise of the specimen afterward do not spoil the measurement. For the successive measurements, however, it is necessary to make the temperature-recovery as quick as possible, helium gas is filled in the inner pipe for heat-exchange. In order to fill the heat-exchange gas in the light pipe, a window should be necessary, as shown in Fig. 5. At the present experiment, a Si window or a crystal-quartz window[19] is used.

iii) High field magnet

The main part of the magnet is made by cutting out a helicoid of 33 turns from a Cu-2%Be block (45 mm in diameter × 300 mm in length) and by subsequently heat-treating it. The dimension of the magnet coil is 45 mm O.D., 13.6 mm I.D., and the thickness of one-turn plate is 1 mm. The photograph of the magnet is shown in Fig. 7. Several ten plates of thin doughnut shape were cut from a large Myler sheet of 100 μm thickness and were joined in series to a spiral. They were employed for insulation between plates of the helicoid. The points for which particular attentions were paid in the construction of the magnet are; (1) a tight fastening between the coil and the electrodes in order to prevent sparkings at the slight gap often produced by a large current flow, (2) holding an end of the 12mm$^{\phi}$ stainless-steel pipe by bellows to protect the pipe-system from a vacuum-break due to the differences of the

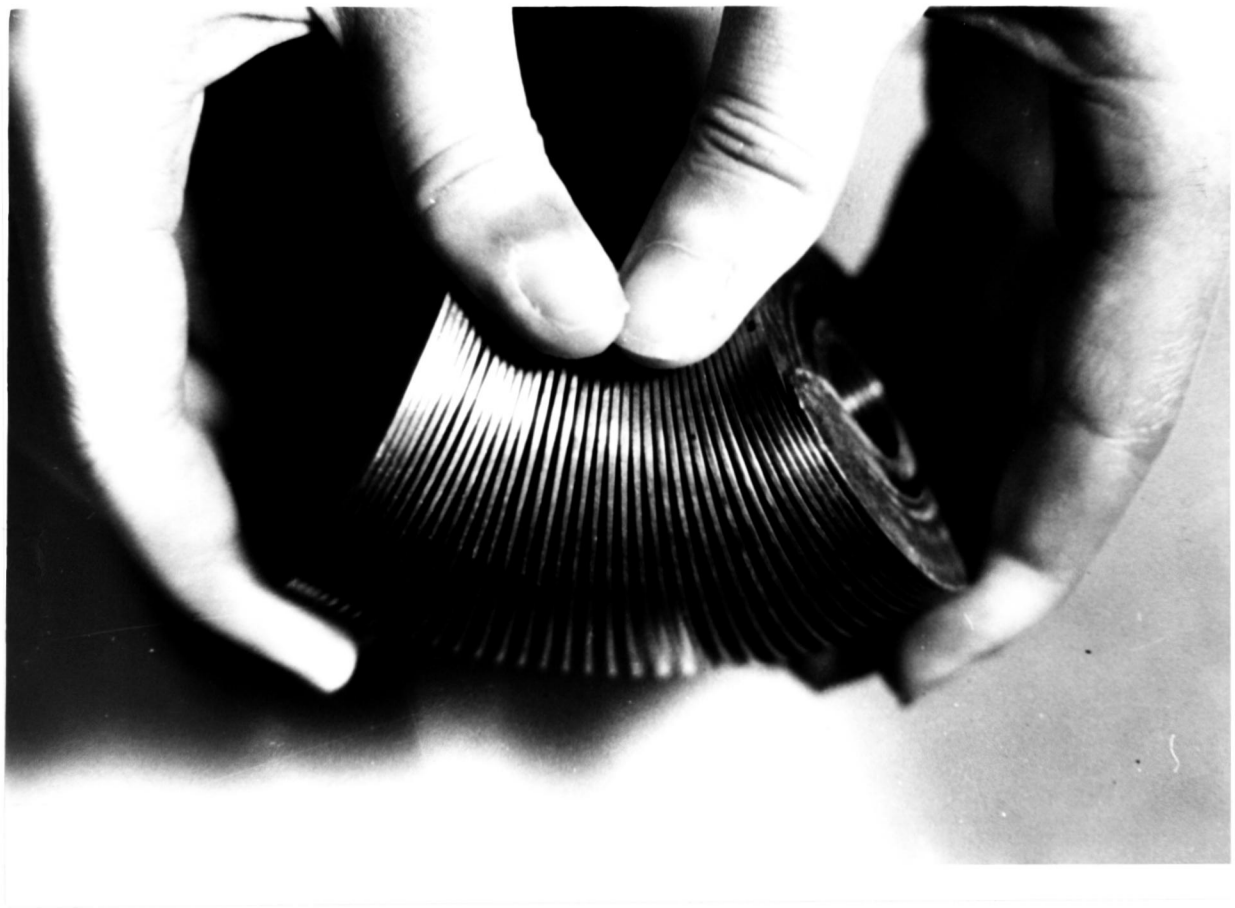

Fig. 7. Photograph of the helical coil of the electromagnet cut from a Cu-2%Be block; the O.D. is about 50 mm.

expantion coefficients of employed materials or due to high magnetic field shock,

(3) making paths to put out the enormous bubbles produced in vaporization of liquid nitrogen at the energy consumption of the intense pulsed magnetic field.

2.3.3. Time interval adjuster and power supplies

The schematic diagram of the time interval adjuster and the power supplies is shown in Fig. 8.

In the lower part of the figure, the power supply for the magnet is illustrated. The voltage E_0 charged in the condenser C of 1500 μF, which comes up to 3.4 kV at the maximum, is divided by resistors into one-twelfth, E_0', and is compared with a variable standard voltage E_s at the comparator circuit. The condenser is charged up just to $E_s = E_0'$.

The time interval adjuster shown in the middle part of the figure is prepared for making time delays and triggers required for the time schedules shown in Fig. 2.A, B, and C.

2.3.4. Boxcar integrator

In the preliminary experiment, we get the transmittance as the ratio of the peak outputs of Golay cells, I to II, by reading on an oscilloscope. However, this method is not applicable neither to the transmission measurements of weak intensity nor to the requirements for raising efficiency of the measurements. In the present experiment, the boxcar integrators are used to integrate the pulsed output, v_1 and v_2 from the Golay cells, I and II during the time interval $t_4 \sim t_5$ (shown in Fig. 2), thus the integrated voltages v_1 and v_2 are held as d.c. outputs, V_1 and V_2 of the integrators. Consequently, the ratio of V_2 to V_1 given by the divider represents the transmittance of the specimen in a fixed magnetic field. Actually, about ten or more than

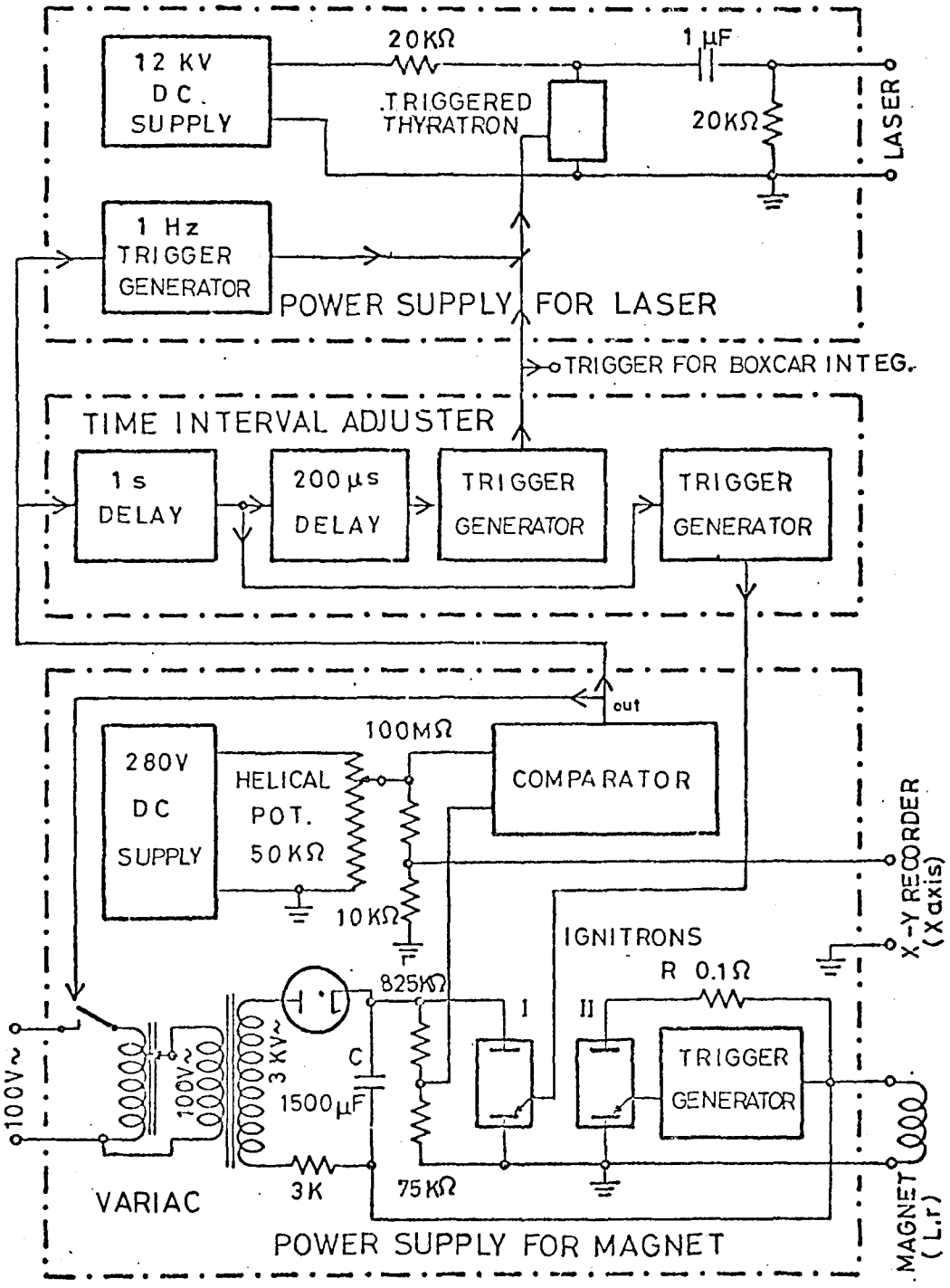

Fig. 8. Block diagram of the time-interval adjuster (the middle part), the power supply for the laser (the upper part), and that for the magnet (the lower part).

ten pulses are integrated for each fixed magnetic field to improve the S/N ratio. The output voltage of an integrator is represented by

$$V = \text{const.} \times \sum_{i=1}^{n} \int_{t_{i4}}^{t_{i5}} v_i(t)dt \ , \qquad (2.1)$$

where i means the i'th pulsed output, n the number of integrated pulsed signals (10 $\sim$ 20) and $(t_{i5} - t_{i4})$ = constant $\sim$ 10 msec. The interval between succesive pulsed signals, t_{i+1} and t_i, is mainly determined by the charging time of the condenser for the magnet and is in a range of 4 $\sim$ 50 sec. Therefore the output voltage of the integrator should be free from a time decay during the operation, occasionally over ten minutes in the case of the maximum field. Accordingly, the holding time has to be as long as at least one hour in spite of the short integrating time of about ten milliseconds.

The full-circuit diagram of the integrators is shown in Fig. 9, and a block-diagram for explaining the operation is indicated in Fig. 10. A signal from the Golay cell is amplified at the preamplefier (a) with a gain controller. The gate pulse shaper (b) makes a gate pulse signal by receiving a trigger pulse from the time interval adjuster. And the gate (c) is opened during the gate pulse is applied for transmitting the amplified signals to integrate in the mirror integrator (d).

On the other hand, a high induction noise caused by the laser and the magnet is particularly mixed into the signals during the first 1 msec. Thus the gate was designed to close in this time, and the amplification system has to be perfectly shielded from electrical induction.
A rectangular pulse width of Fig. 2E is controled by M-1 and M-2 (in Fig. 9) corresponding to t_5 and t_4, respectively.

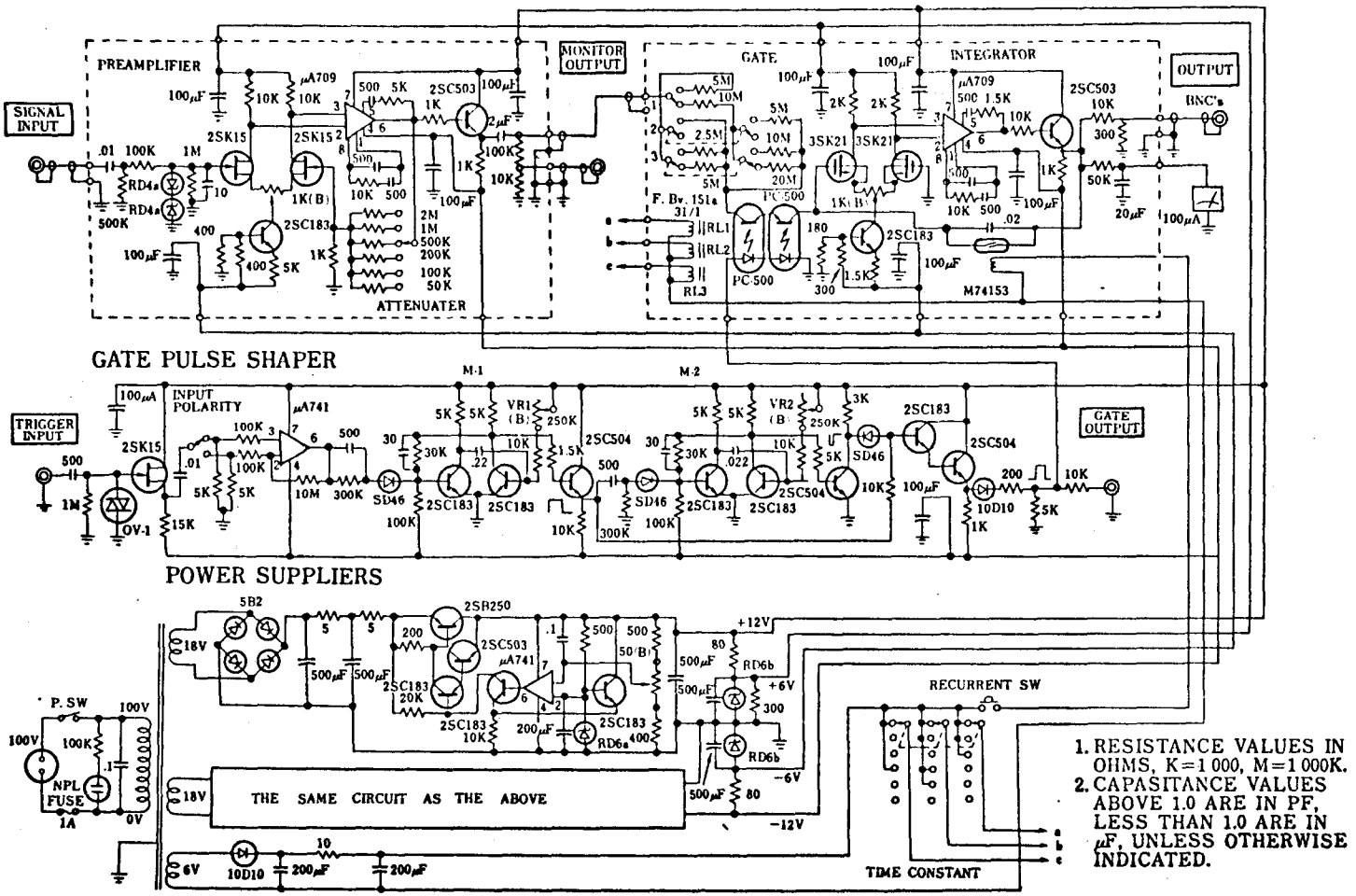

Fig. 9. Full-circuit diagram of the boxcar intergrator and attached circuit.

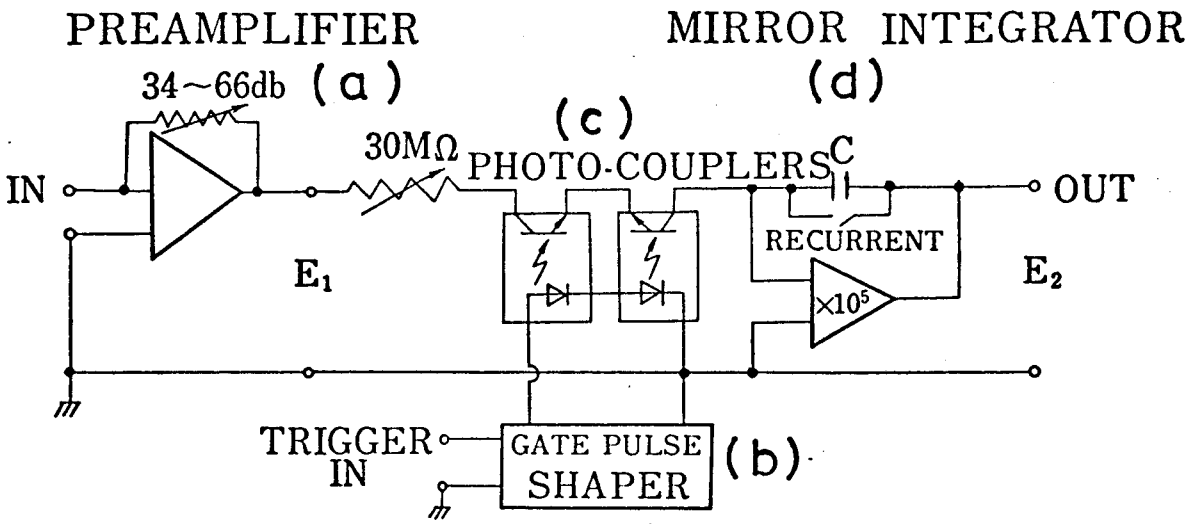

Fig. 10. Block diagram for explaining the operational mechanism in selection and accumulation of the signals.

For the gate, we use, as the pioneers, two photo couplers, each composed by a GaAs luminous diode and a Si photo-transistor. The transistors are employed connecting in series in reversing. With this connection the gate circuit has a resistance of more than 10^{12} Ω without current in GaAs diodes, while, the resistance drops to less than 10 KΩ by flowing current of about 10 mA in the luminous part.

Let us first consider a mirror integrator circuit with a gate switch as indicated in Fig. 11. The output voltage E_2 is related to the input voltage E_1 with the following formula:

$$E_2 = \frac{1}{CR}\int_{\substack{\text{gate}\\\text{open}}} E_1 dt + \frac{1}{CR_r}\int_{\substack{\text{gate}\\\text{close}}} E_1 dt - \frac{1}{|A|CR}\int_{\substack{\text{gate}\\\text{open}}} E_2 dt - \frac{1}{|A|CR_r}\int_{\substack{\text{gate}\\\text{close}}} E_2 dt, \quad (2.2)$$

where $|A|$ is an amplification factor and R_r is a leakage resistance of the gate closed. On the condition that E_2 is same order to E_1 and $|A| \gg 1$, the third term in the right-hand side can be neglected, and moreover, the second term becomes very small when E_1 never contains d.c. component. Thus the expression (2.2) simplified to

$$E_2 = \frac{1}{CR}\int_{\substack{\text{gate}\\\text{open}}} E_1 dt - \frac{1}{|A|CR_r}\int_{\substack{\text{gate}\\\text{close}}} E_2 dt\ , \quad (2.3)$$

The output voltage E_2 increases as $(1/CR)\int E_1 dt$ when the gate is open while it decays with the time constant of $|A|CR_r$ when the gate is closed. Therefore, the increasing rate of E_2 can be controlled by changing the value of CR. CR may be assumed to be about 200 msec on the condition that $|E_1| \sim |E_2|$. The condition can be realized by 20 times repetition of openning the gate in the time interval of 10 msec and after the repetition $|E_2|$ reachs $|E_1|$. It is known from Eq. (2.3) that the decay

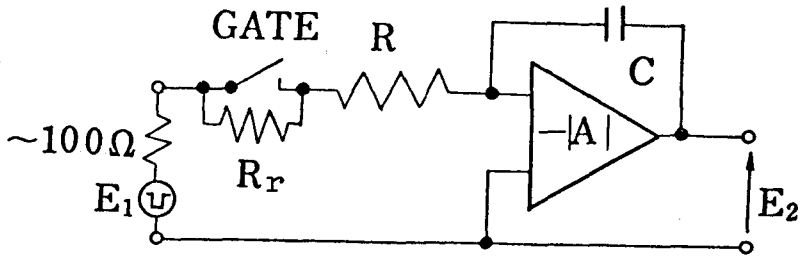

Fig. 11. Schematic diagram for the mirror integrater.

time can be estimated from the products of R_r, C and $|A|$. One may roughly set the time required for holding E_2 constant (named "holding time") as $|A|CR_r/100$. From our conditions of $R_r \sim 10^{12}$ohm, $C = 0.02\ \mu F$ and $|A| \sim 10^5$, the estimated value if the holding time becomes $\sim 2 \times 10^7$sec; i.e., $\sim$ 300 days. However, in the actual circuit the holding time is determined by leakages between drain and gate in MOS FET and by those through capacitor C. Then the holding time often becomes several hours.

It is particularly important that this integrator part should be maintain in a dry atmosphere. For the purpose, we used a vacuum case.

2.3.5. Recording

Both signals from the two boxcar integrators are introduced into a potentiometer part in an X-Y recorder, and the ratios of the signals are plotted as the Y-components. Generally the mechanism of an electronic pen recorder is as follows: the recording pen is moved by a servo-mechanical system which potentiometrically divides a constant voltage V_c as to coincide with the input voltage. In our case of using Y-component mechanism as a divider [20], the constant voltage for the Y-compornent is substituted by the output of signal from the boxcar integrator for reference V_1, while the signal V_2 from the sample is put into the normal input of the Y-component. Thus the Y-component of the recorder operates as a voltage divider and indicates V_2/V_1. On the other hand, the X-component of the recorder is used for giving the magnetic field intensities as is previously described.

2.4. Operations

In the present measurement, it is necessary to confirm that the magnetic field is linear to the voltage of the charged condenser. This certification was done by using a search coil and the result is shown

in Fig. 12. Moreover, the calibration of the magnetic field as a function of the condenser voltage was carried out by measuring the cyclotron resonance for n-Ge (111) and n-Si (110) by means of the present spectrometer, and the results are also shown in Fig. 12.

In the above mentioned experimental procedures, we emphasized the importance of accurate apparatus, but the thickness of the specimem is another important point for getting the true information of the absorption line. Because the change of transmission saturates for $\alpha d > 3$ (α is a absorption coefficient and d the thickness) in transmission spectra, and a small change of the transmission signal in the vicinity of a resonance region is often screened by the signal fluctuation. The above troubles in the measurement are shown in Fig. 13, namely the line shape changes as the thickness increases from 60 μm to 500 μm. The true information can be given from transmission lines of the specimens of 60 and 90 μm in thickness. Therefore, it is necessary to change the thickness of the specimen according to the number of free carriers, generally which is changed on a large scale by the temperature.

2.5. Samples

The samples (n-CdS) used in this experiment had a carrier concentration of 1×10^{16} cm^{-3} and a mobility of about 2180 cm^2/Volt sec at 77 K. This is shown in Table 1. The samples are etched by 2-N HCl for about 30 minutes after being cut into discs. The samples are prepared in a high pressure Tammann furnace and kindly offered to us from Teikoku-Tsushin Kogyo, Inc.

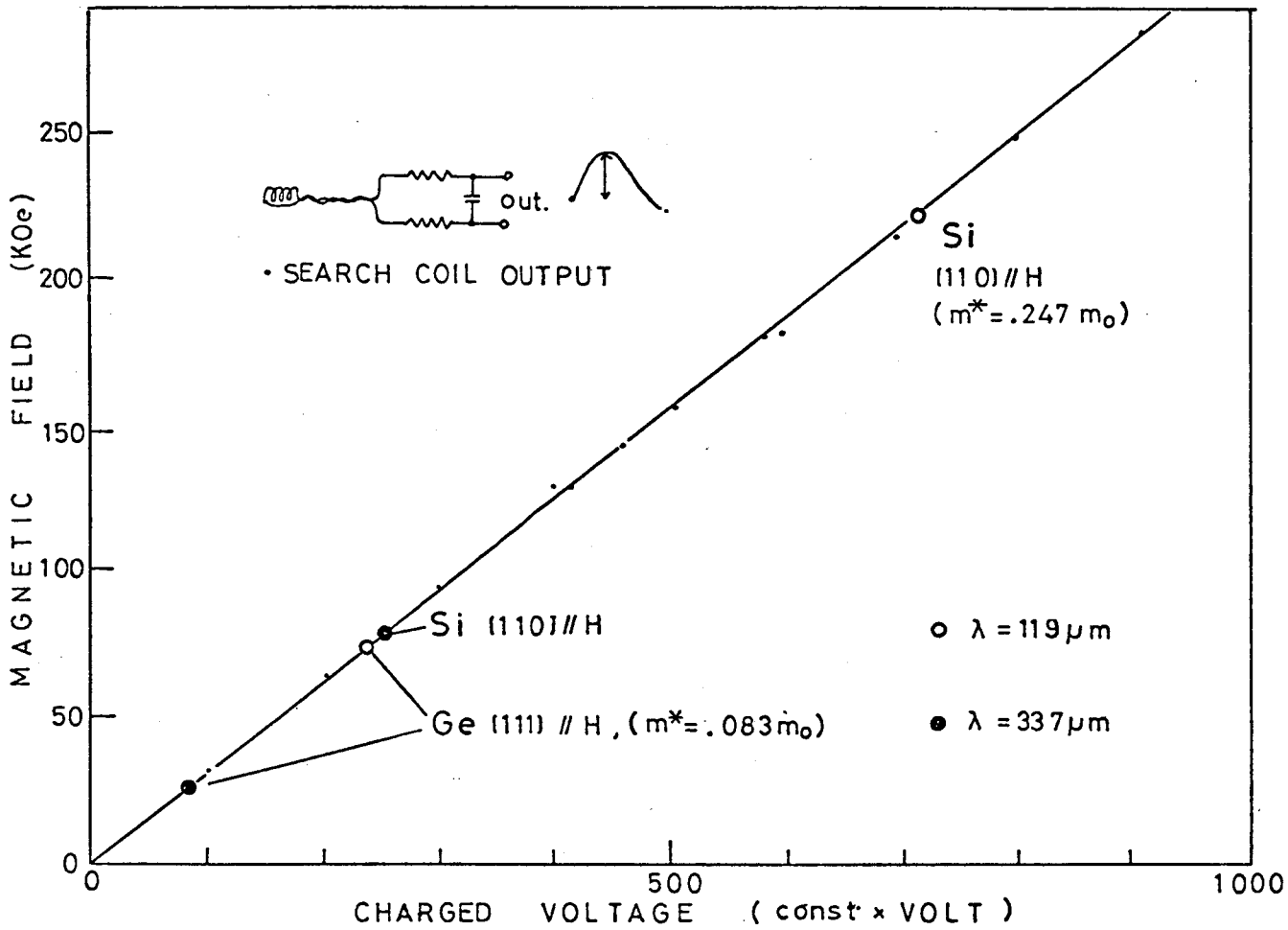

Fig. 12. Magnetic field calibration. The magnetic field measured is linear to the charged voltage of the condenser bank.

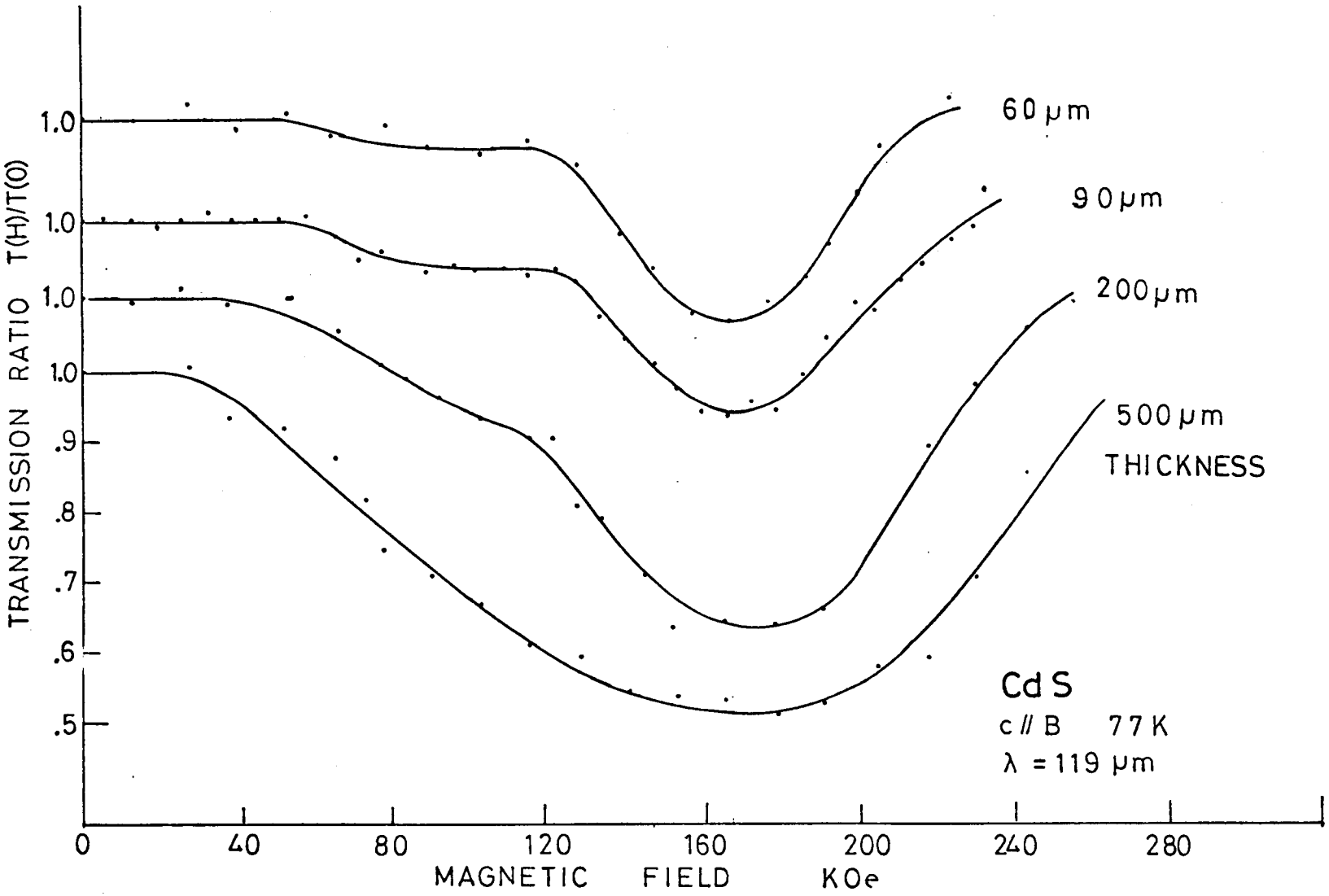

Fig. 13. Effect of the sample thickness upon the transmission spectra of the far-infrared cyclotron resonance in CdS.

Table 1. Characteristics of the sample

		N_C (cm^{-3})	μ (cm^2/Vs)
n-CdS	77 K	2.18×10^{15}	2180
	294 K	1.03×10^{16}	298

3. EXPERIMENTAL RESULTS

The electron cyclotron resonance of n-CdS was observed at the wave length of 119 μm by using an H_2O laser. Fig. 14 shows the transmission ratio T(H)/T(0) versus the magnetic field at various temperature measured by using circular polarized radiation. The magnetic field was applied parallel to the c-axis of CdS crystals and also parallel to the incidence. The sample used had the carrier concentration of $1x10^{16}cm^{-3}$ at 300 K. However, at lower temperature the effective carrier concentration greatly decreased with temperature. Therefore, four kinds of specimens different thickness were prepared to satisfy the condition, $\alpha d < 3$, namely 90, 200, 500 and 3060 μm.

It is to be noted in Fig. 14 that the main peak at about 165 kOe shifts to higher magnetic field side with increasing temperature below about 50 K, while it does not change above the temperature, in other words, the effective mass becomes heavier by raising temperature in the temperature range below 50 K.

A sub-band is found in the lower field side about 85 kOe, and this position seems independent of the temperature.

In measurements of cyclotron resonance, we can make clear the selection rule of cyclotron resonance absorption to use a circular polarized light together with changing the direction of the magnetic field, which is decided by the direction of current in magnet-coil. And also by using circular polarized light, it is possible to improve the S/N ratio, because we can remove the light independent of the resonance absorption by the method. A circular polarized light was obtained by employing a circular polarizer made of a linear polarizer and a quarter-wave plate. As shown in Fig. 5, the polarizer was set just before the specimen. An X-cut crystal quartz plate was used for the quarter-wave

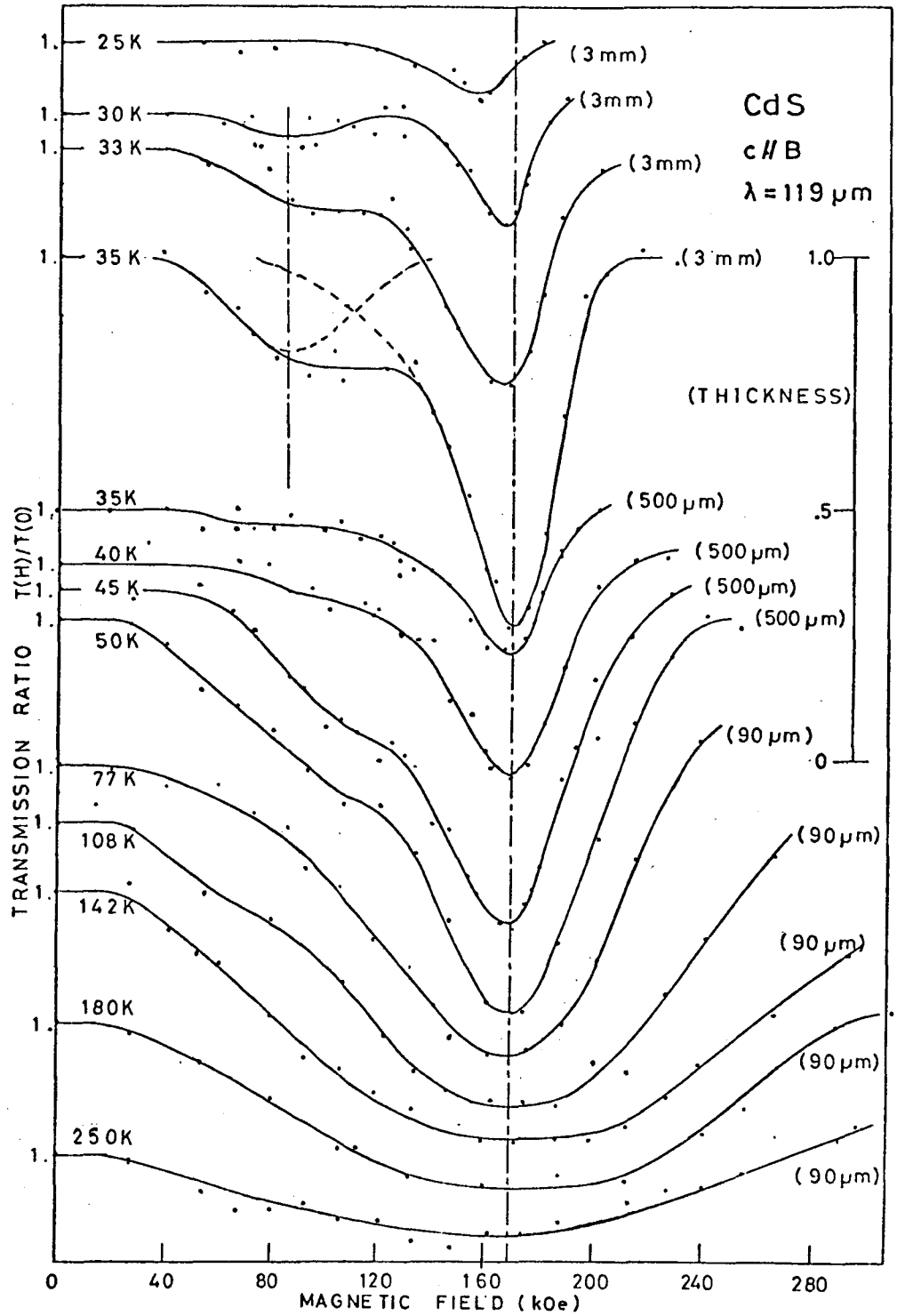

Fig. 14. Transmission ratios, T(H)/T(0), as functions of magnetic field at various temperatures. A circulary polarized light was used.

plate of 600 μm in thickness.

The spectrum of the inactive side of the electron cyclotron resonance (hole polarity) is shown in Fig. 15. In the figue, the active side (electron polarity) spectrum is also shown in comparison. Both side spectra have same spectral figure, though the absorption intensities are appreciably different. From the above experimental results, it may be concluded that the main-peak and sub-band are only active to the same polarization. Thus, the absorption in inactive side is believed to be caused by a mixing of right circular polarized light with left one, which results from the incompletion of the polarizer. The mixing rate can be estimated to be about several percents from Fig. 15.

The cyclotron resonance in CdS at 337 μm is shown in Fig. 16. As the relaxation time at the temperature (35 K) is not large enough to satisfy the condition $\omega_c\tau >> 1$ (ω_c is the angular resonance frequency, τ, the time between collisisions), the line shape for 337 μm is seen to appreciably broaden, though the peak point is estimated to be 56 kOe, and the cyclotron effective mass is calculated to be $0.175m_o$. This result suggests that the cyclotron mass must depend on the magnetic field.

Through the above mentioned, we have paticuraly interested in

(1) the effective mass shift below 50 K and stand-still above 50 K,

(2) the sub-band at about 85 kOe, and

(3) the magnetic field dependence of the effective mass.

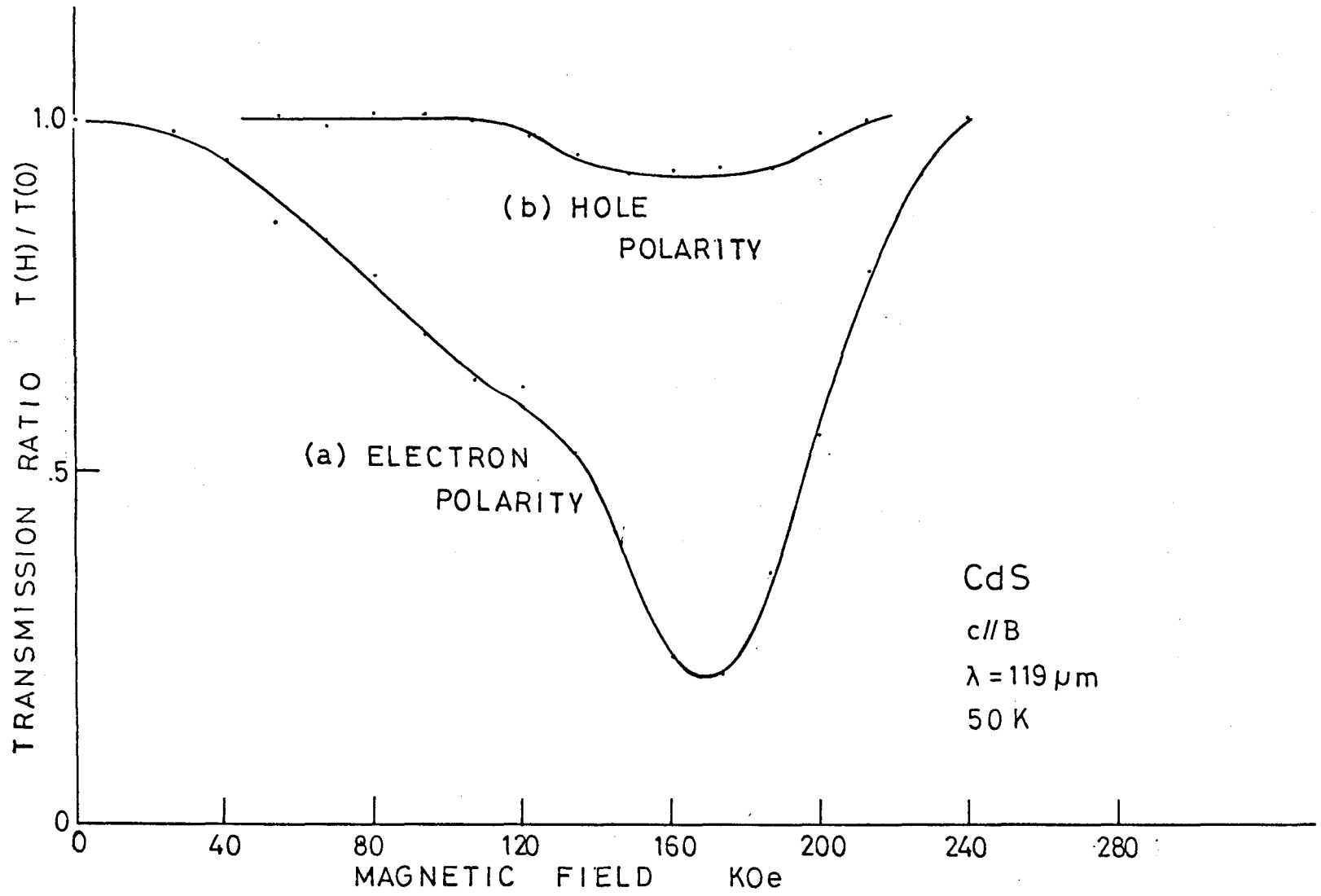

Fig. 15. Cyclotron resonance spectra in CdS at 50 K by left and right circularly polarized radiations.

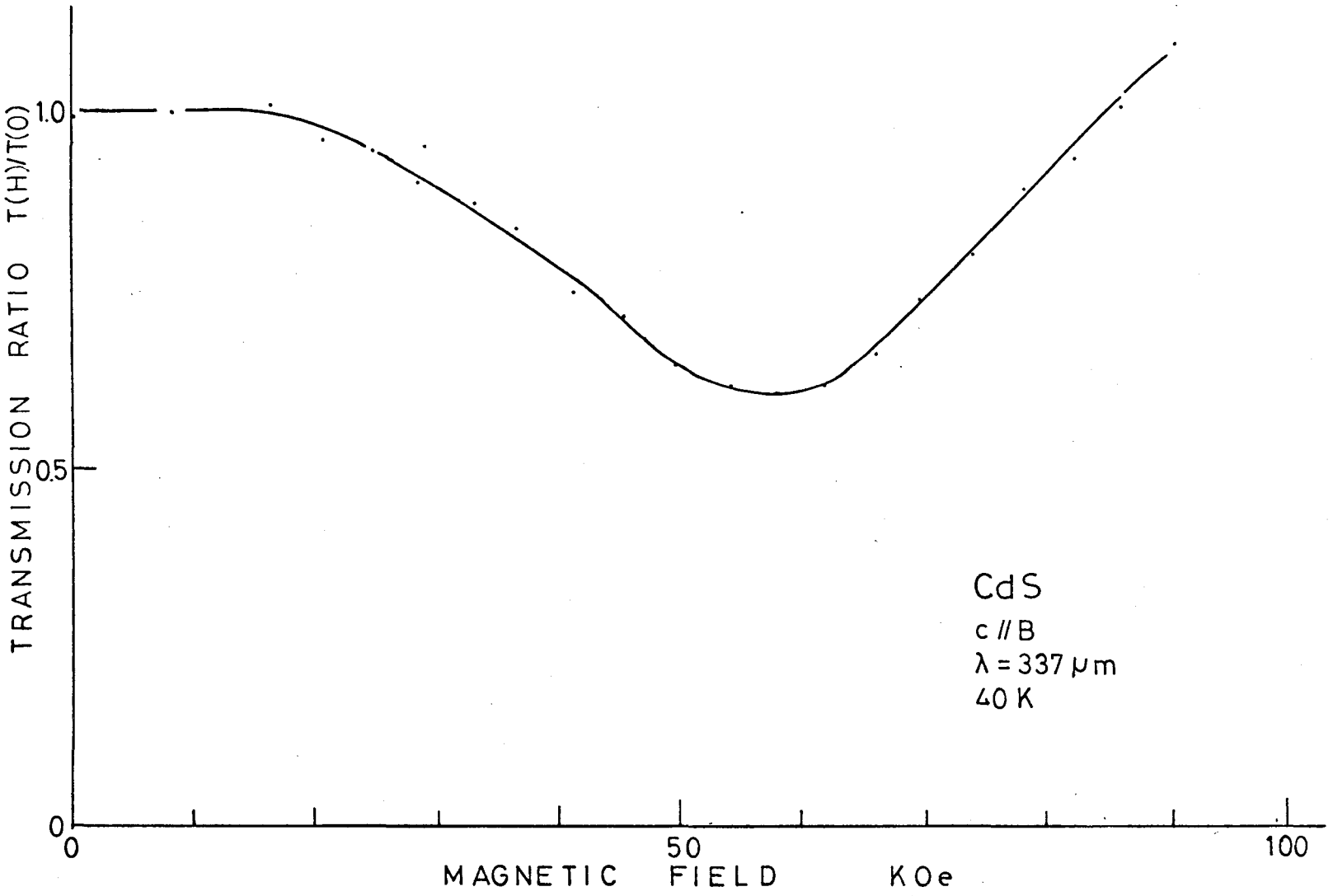

Fig. 16. Cyclotron resonance at 337 μm.

4. COMPARISON WITH THEORIES

4.1. Introduction

The piezoelectric polarons effect has been considered to play an important role on the cyclotron mass shift in CdS. And the mass shift takes place as functions of temperature and magnetic field. For explaining the dependence of the cyclotron effective mass and the relaxation time on temperature, many different expressions were predicted by many investigators, some of which are shown in table 2. These formulae were derived from the same basic Hamiltonian,

$$\mathcal{H} = \frac{\left(p + \frac{e}{c} A \right)}{2m} + \sum \hbar s q \, b_q^+ b_q + \text{const.} \times \sum \frac{1}{\sqrt{q}} \left(b_q + b_{-q}^+ \right) e^{iq \cdot r}, \tag{4.1}$$

where e is the elementary charge, c the light velocity, A the vector potential, m the electron band mass, b_q and b_q^+ are annihilation and creation operators for phonons of wave number q, respectively, and s the velocity of sound. The derivation of this equation is shown in Appendix I. We can see in the table that considerable inconsistencies for the solution of Eq. (4.1) exist among them as the results of the differences in their methods of approximations. The energy of the piezoelectric polarons under the zero magnetic field was studied by Mahan and Hopfield[9], Porsch[21] and Okamoto[22]. Mahan and Hopfield calculated it by means of the second order perturbation theory, Porsch's result was obtained by a Green's function method and Okamoto's by a variational method. Mahan and Hopfield predicted that the piezoelectric polaron mass (m*) is always smaller than the bare band mass (m) and m* is a increasing function of temperature. On the contrary, Porsch and Okamoto predicted that m* is always larger than m, and moreover, Porsch's

Table 2. Theoretical results of polaron mass shift and line width due to piezoelectric interaction

	magnetic field H	bare band mass m and piezoelectric polaron mass m*	mass shift $(m/m^* - 1)$	half line width $\Delta H / H$
Mahan-Hopfield[9]	0	$m > m^*$	$T^{-1/2}$	—
Porsch[21]	0	$m < m^*$	$(\frac{m^*}{m} - 1) \propto T^{-2}$	—
Okamoto[22]	0	$m < m^*$	—	—
Miyake[13]	finite	$m > m^*$	$T^{2/3} H^{-1}$	
Saitoh-Kawabata[11]	finite	$k_B T/\hbar\omega_c \leq 0.4$ $m \leq m^*$ $k_B T/\hbar\omega_c > 0.4$ $m > m^*$	increasing function of T	$T^{1/2}$

result indicated that m* would decrease with temperature. In the quantum limit condition ($\hbar\omega_c >> k_BT$), Miyake[13] and Saitoh-Kawabata[11] calculated the temperature dependence of the cyclotron mass and the line width. A thermal Green's function method was employed by Miyake and the calculation by Saitoh and Kawabata was started from the Kubo formula for the conductivity. Both theories indicate that the piezoelectric polaron mass should decrease with temperature and the half line width should broaden in proportion to $\sqrt{T}$.

Considering that the present experimental results were measured in the condition; $\hbar\omega_c > k_BT$. We will compare the experimental results with the theory of the quantum limit proposed by Miyake (Appendix II) in the following sections.

4.2. Line width

The half line width of the cycloton resonance spectrum theoretically derived by Miyake is given by Eq. (A.41), which is

$$\frac{\Delta H}{H^*} \sim 1.5 \sqrt{\lambda} \ ,$$

$$\lambda = \sqrt{2} \ \alpha \ (\ell / a_B) \ (k_B T / \hbar\omega_c) \ . \qquad (4.2)$$

where H^* is the resonant magnetic field, α the square of electromechanical coupling constant, ℓ the lowest Landau orbit radius, a_B the effective Bohr radius in the crystal, and ω_c the cyclotron resonant frequency.

Using the numerical values; $\hbar\omega_c$ = 10.5 meV, $a_B \sim 25$ A, α = 0.035, and $\ell \sim 60$ A, we can obtain the half line width as,

$$\frac{\Delta H}{H^*} \sim 4.8 \times 10^{-2} \sqrt{T} \ . \qquad (4.3)$$

On the other hand, the half line widths obtained by the experiments are shown in Fig. 17. We can see that the half line width increases in proportion to $\sqrt{T}$ below 50 K, and steeply rises above 70 K. The behavior below 50 K is attributed to a scattering mechanism by the piezoelectric field accompanied by acoustic phonons and that above 70 K is to another scattering mechanism by optical phonons.

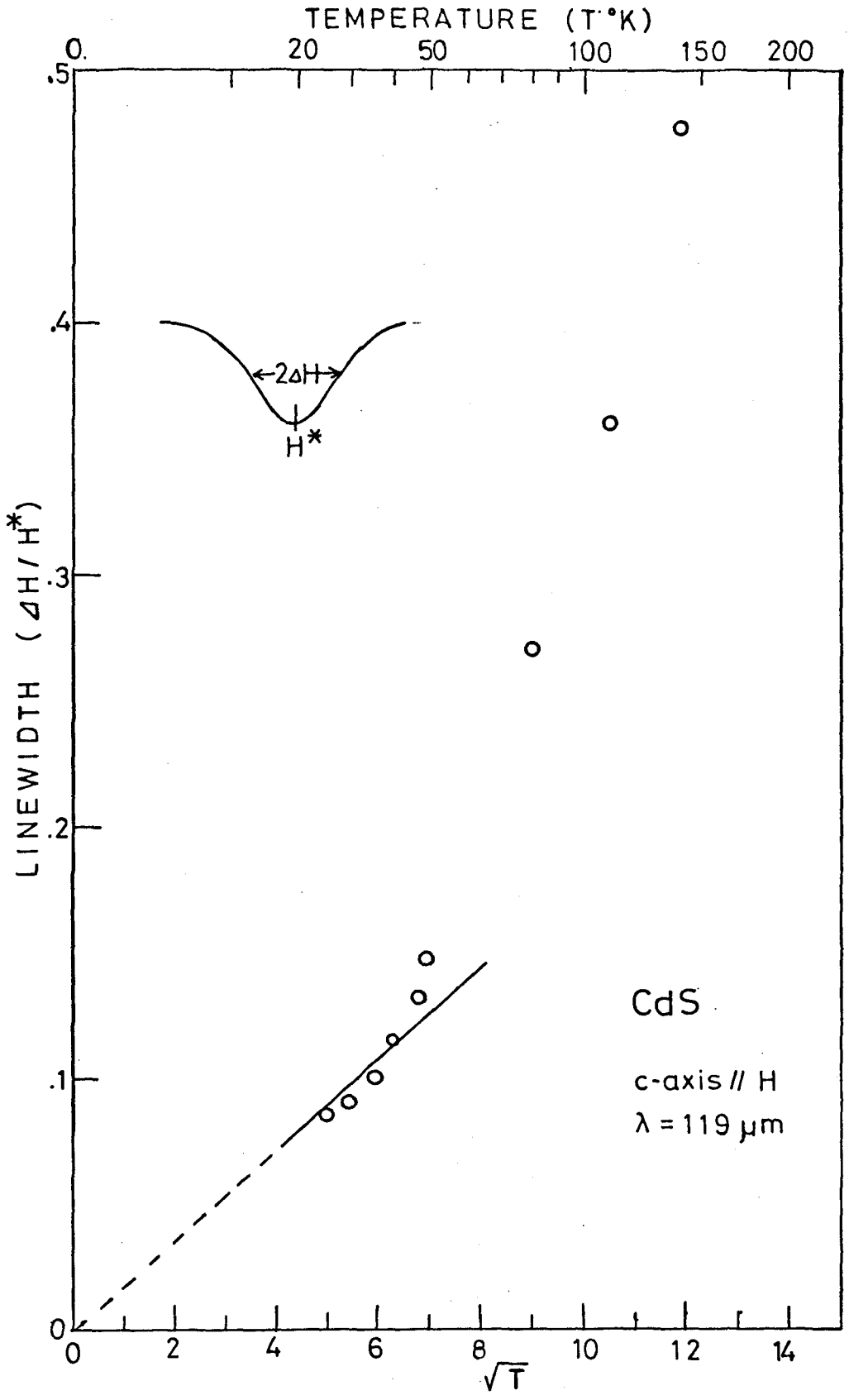

Fig. 17. Plots of the half line width of the resonance curves vs. $\sqrt{T}$. The solid straight line indicates that $\Delta H/H^* \approx 1.8 \times 10^{-2} \sqrt{T}$

4.3. Cyclotron mass shift

The theoretical mass shift is given by Eq. (A.43), that is

$$\frac{m}{m^*} - 1 \sim 0.18\,\lambda^{2/3} \propto T^{2/3} H^{-1} . \qquad (4.4)$$

This equation indicates that the piezoelectric polaron mass decreases with temperature and increases with magnetic field.

Assuming the bare band mass to be 0.19 m_o, we may have the temperature dependence of the piezoelectric polaron mass shift, as shown in Fig. 18 by the dotted line.

On the other hand, the experimental result indicates that the cyclotron resonance electron effective mass increases with temperature at 119 μm, as shown in Fig. 18 by the solid line, and this mass decreases about several percents when the radiation wave length is increased from 119 μm to 337 μm. That is; the experiment contradicts to the theory about the temperature dependence of the cyclotron mass, but it agrees for the magnetic field dependence of the mass.

It is supposed that the contradiction in mass shift is originated from the assumption that the electron couples only piezoelectric field accompanied by the acoustic phonons.

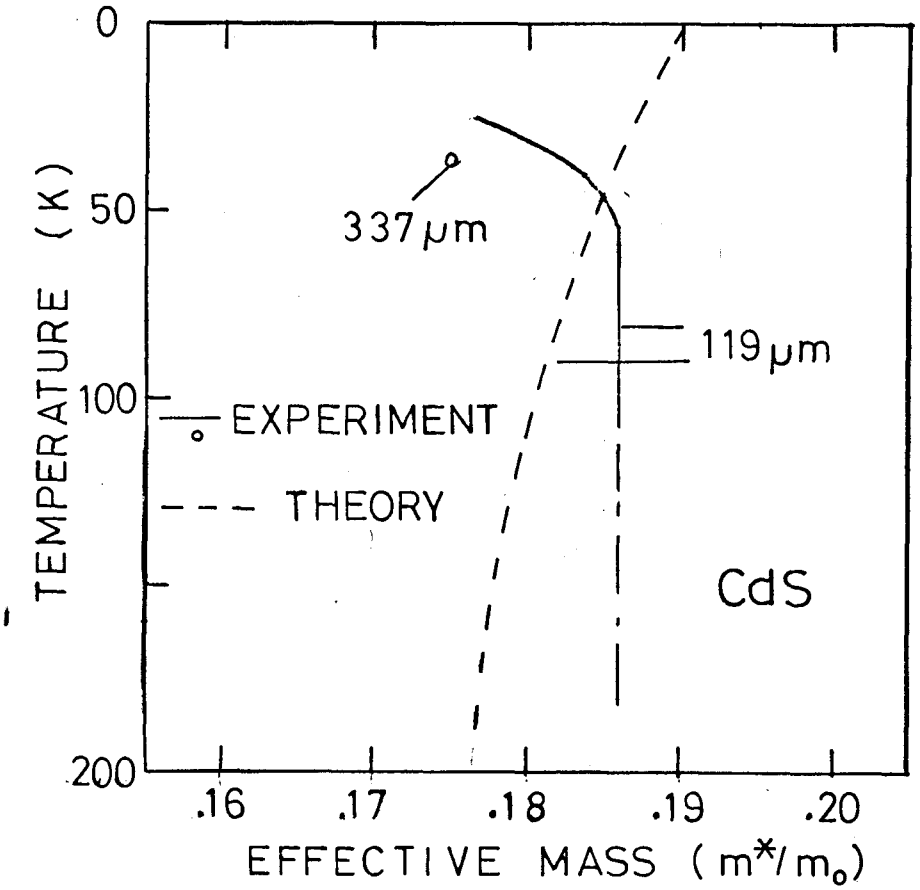

Fig. 18. Temperature dependence of mass shift.

----- theoretical mass shift in which the bare band mass of CdS of 0.19 m_o is assumed.

——— experimental mass shift.

5. DISCUSSION

Recently the phonon branches of CdS have been known more clearly on account of the development of the Raman spectroscopy[23]. The lowest energy optical phonon was found out to exist at 43 cm^{-1} (5.3 meV). The optical phonon has a possibility to affect the electron motion together with the accoustic phonon in the temperature range below about 100 K. On the other hand, the lowest optical phonon branch is considered to be the vibration mode having Γ_6 symmetry according to the theory of the band structure calculation. Fortunately, the Γ_6 vibration mode is one of the Raman active mode, and was able to be found in the Raman spectroscopy. That is, this mode will make the longitudinal polarization wave accompanied by the optical phonon (43 cm^{-1}). Therefore, it is natural to consider that the electron in CdS receive an effect from the optical phonon.

(i) Cyclotron-phonon resonance[24]

Let us consider a cyclotron resonance measurement by far-infrared radiation of the energy $\hbar\omega$ = 10.5 meV (λ = 119 μm). The cyclotron resonance peaks should appear at the position, where one of the following relation is satisfied, apart from the ordinary cyclotron resonance peak at $H = m^*c\omega/e$.

$$H_1 = \frac{m^*c}{\hbar e}(\hbar\omega - \hbar\omega_0) , \qquad (\hbar\omega_c' = \hbar\omega - \hbar\omega_0) , \tag{5.1a}$$

$$H_2 = \frac{m^*c}{\hbar e}(\hbar\omega + \hbar\omega_0) , \qquad (\hbar\omega_c'' = \hbar\omega + \hbar\omega_0) , \tag{5.1b}$$

where ω_0 is the angular frequency of the phonon, and Eq. (5.1a) is related to the phonon emission and Eq. (5.1b) is the phonon absorption. Then, at the sufficiently low temperature ($n_q << 1$, where n_q is the phonon number; $n_q = \{\exp(\hbar\omega_0/k_BT)-1\}^{-1}$), only the phonon emission band may appear in the cyclotron resonance spectra and the phonon

absorption band may not be obtained until the temperature becomes high enough ($n_q >> 1$).

The typical cyclotron resonance spectrum with a sub-band is shown in Fig. 19. In the figure, a fairly strong absorption band is found at about 85 kOe which corresponds to the energy, 5.3 meV. Taking into account the lowest energy of the optical phonon being 5.3 meV, it can be seen that the agreement between the experiment result and the energy introduced from Eq. (5.1a) where $\hbar\omega_c' = \hbar\omega - \hbar\omega_0 = (10.5 - 5.3) = 5.2$ meV is fairly well, and the relation is schematically shown in Fig. 20. Moreover, it can be known from Fig. 20 that, when 337 μm far-infrared radiation is used for the cyclotron resonance, the sub-band should not be found at lower magnetic field than the main peak. Surely the experiment at 337 μm, we could not find any sub-band but the main peak, as confirmed from Fig. 16.

(ii) Line width

The relaxation time τ due to the optical phonon (43 cm^{-1}) is theoretically given by

$$\frac{1}{\tau} \propto \frac{1}{\sqrt{T}\ \{\exp(43hc/k_BT) - 1\}} \qquad (5.2)$$

The dependence of $1/\tau$ on the temperature T from the relation (5.2) is drawn in Fig. 23, while the half line width obtain from the experiment result is plotted in the same figure, from the reason that the width is considered to relate to the inverse relaxation time. It can be seen in the figure that the scattering mechanism in the temperature range from 40 K to 100 K is mostly related to the optical phonon of 43 cm^{-1}.

It can be concluded that the electron scattering in CdS above 40 K is mainly due to the optical phonon of 43 cm^{-1}. This mechanism has

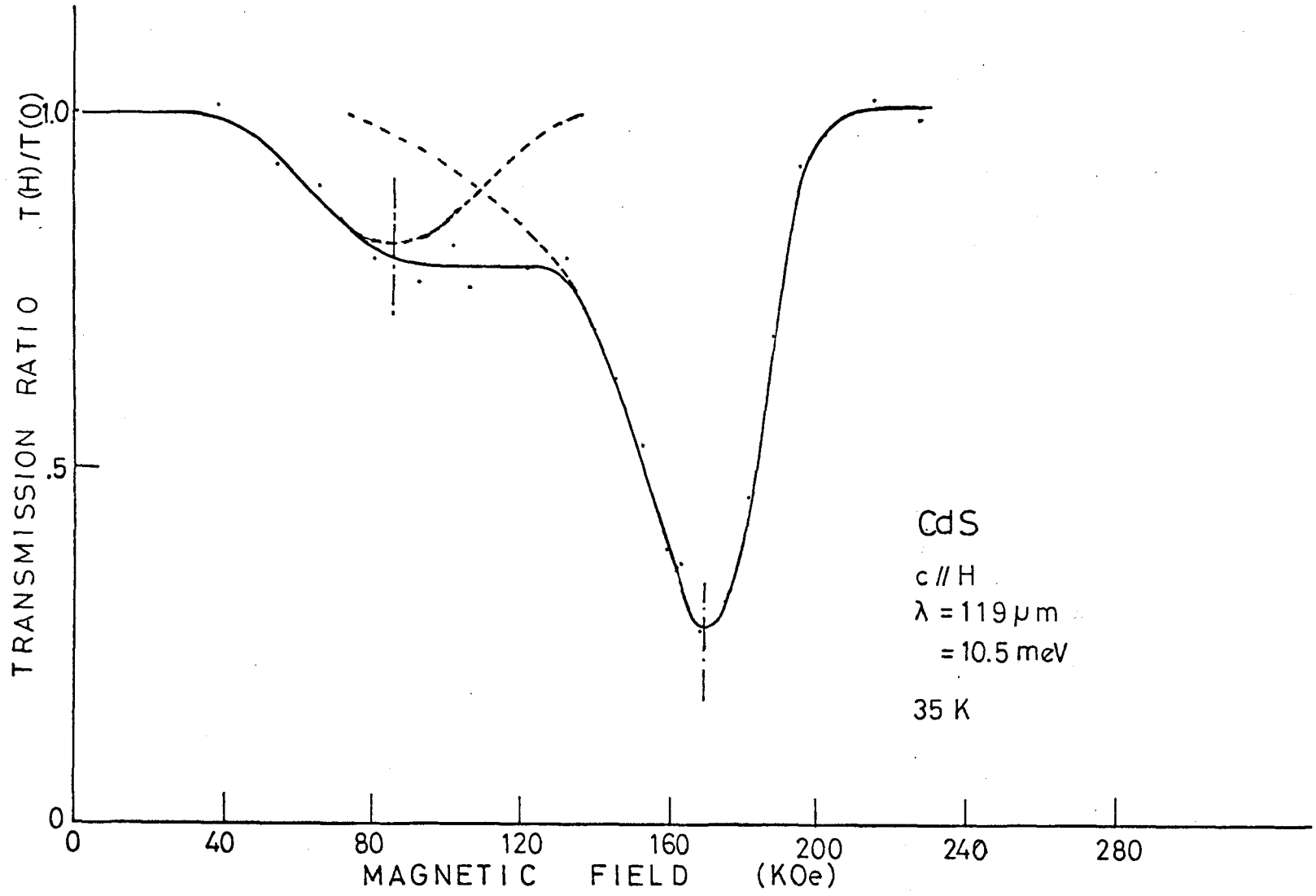

Fig. 19. Typical cyclotron resonance spectrum with sub-band.

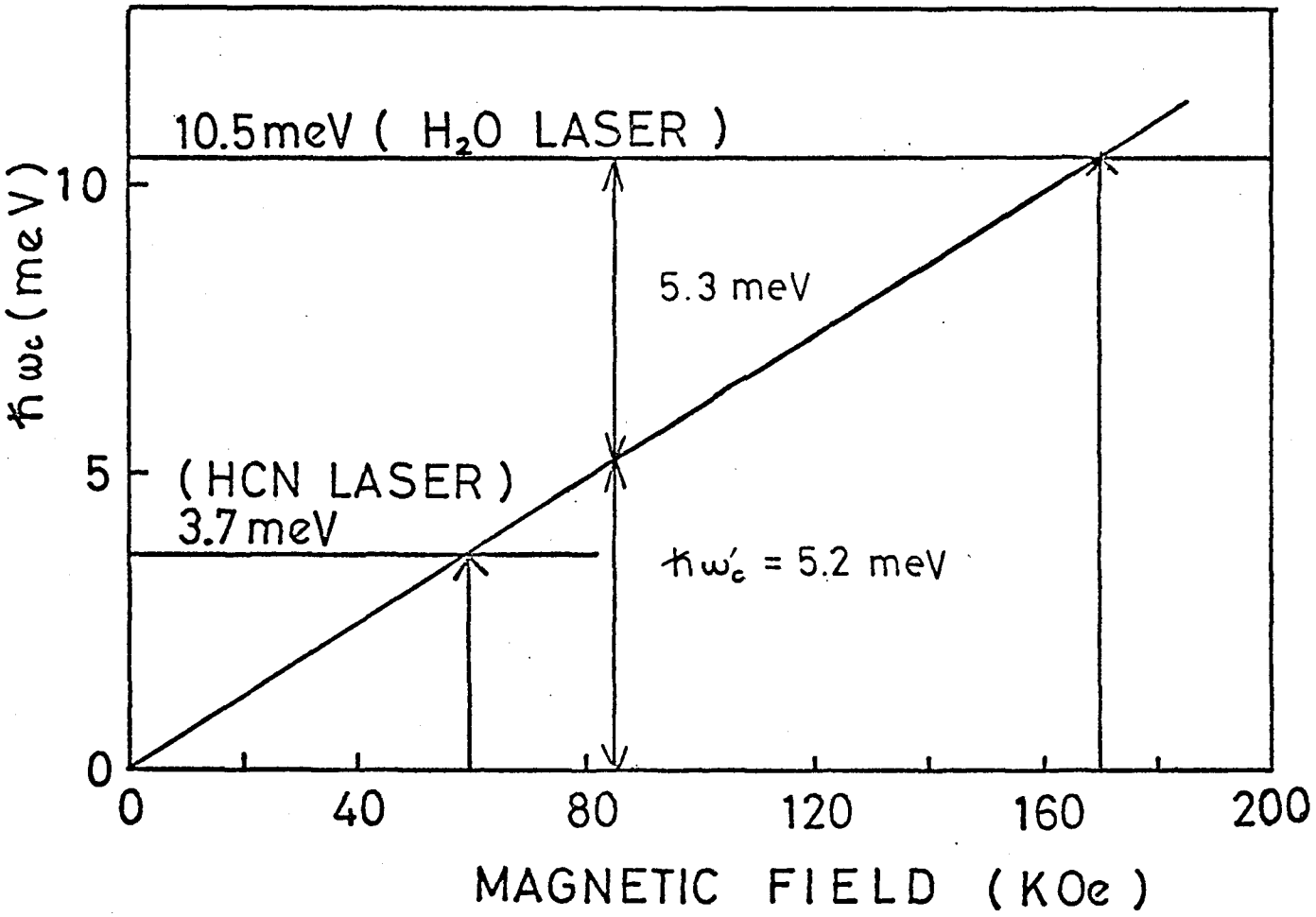

Fig. 20. Schematic energy diagram, indicating the relation between photon energy and magnetic field.

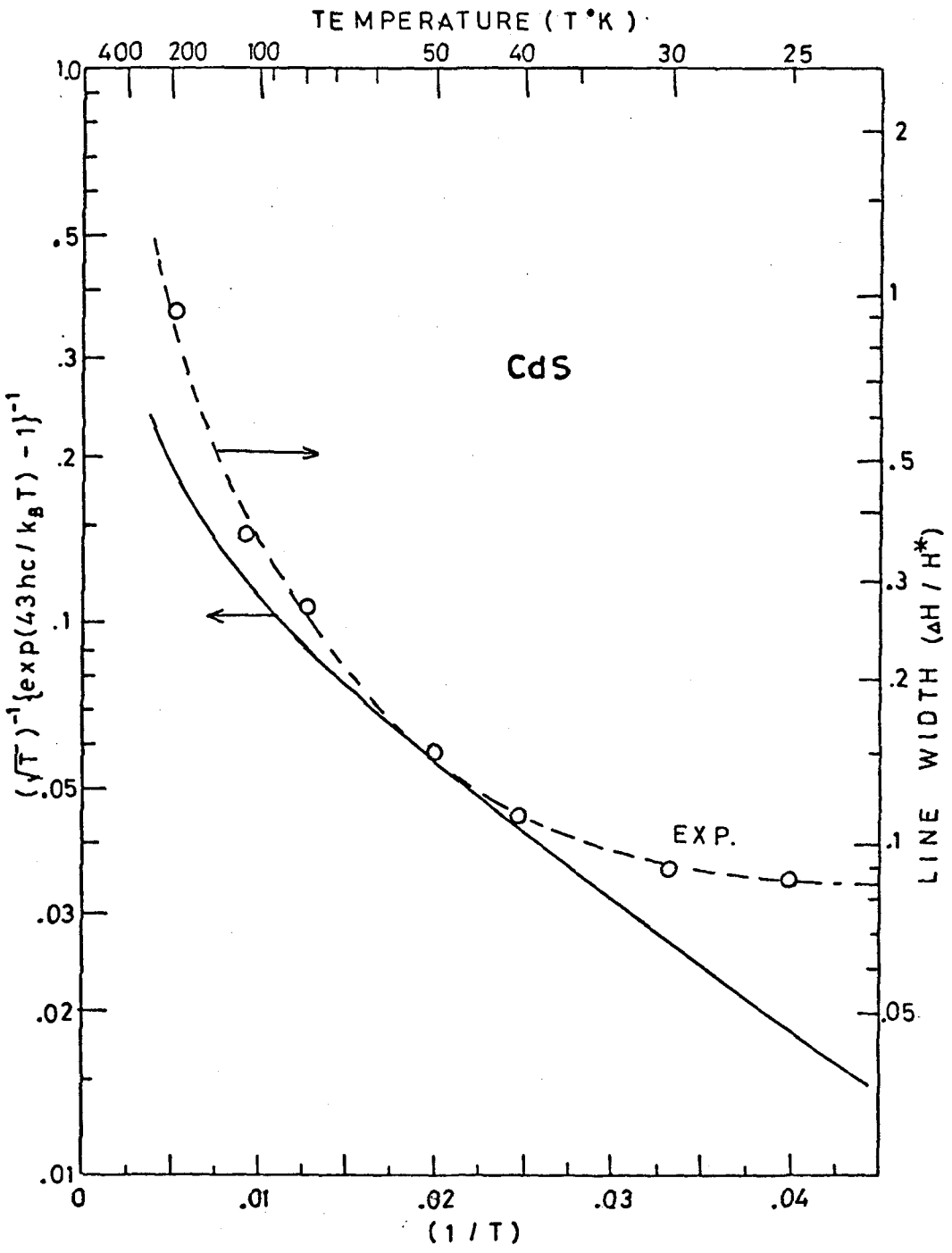

Fig. 21. Theoretical inverse relaxation time and experimental half line width as a function of inverse temperature.

never been given by any other investigators.

Moreover, it may be expected that, by this mechanism, the temperature dependence of the cyclotron mass, the theory of which has had a contradiction with the experimental results, may be explained completely in the near future.

6. SUMMARY

(1) We developed a far-infrared cyclotron resonance spectrometer in order to study semiconductors of low carrier mobility. In the apparatus we utilized pulsed magnetic field (up to 350 kOe) and an H_2O (or HCN) far-infrared laser.

(2) We measured the cyclotron resonance of CdS in the temperature range 25 K $\sim$ 250 K by using the above apparatus, and we obtained the temperature dependence of the line width and the cyclotron mass.

(3) A sub-band appeared in the cyclotron resonance spectra for the H_2O laser of wavelength 119 μm, the position of which was about 85 kOe; the lower field side of the main peak. The sub-band was attributed to the 43 cm^{-1} optical phonon which was observed recently in the Raman spectral analyses.

(4) The temperature dependences of the cyclotron mass shift and line width and the frequency dependence of the mass in the experimental result were compared with the piezoelectric polaron theories by several investigators. Although the theories could qualitatively explain the temperature dependence of the line width and the frequency dependence of the mass, they could not be applied to the temperature shift of the mass. We consider that the more advanced theory will be needed for the explanation, and in the theory we should take into account the electron-optical phonon interaction as well as the electron-acoustic phonon interaction.

APPENDIX I

For the motion of an electron coupled with phonons in a magnetic field, we take the Hamiltonian $\mathcal{H} = \mathcal{H}_0 + \mathcal{H}_1$, where the unperturbed part is expressed by

$$\mathcal{H}_0 = \frac{(p + \frac{e}{c}A)^2}{2m} + \sum \hbar s q \, b_q^+ b_q \ . \tag{A.1}$$

Here e is the elementary charge, c the light velocity, A the vector potential, m the electron band mass, s the velocity of sound and b_q^+ and b_q are creation and annihilation operators for phonons of wave number q, respectively. For a magnetic field $H = [\ 0,\ 0,\ H\ ]$, the Landau gauge $A = [\ 0,\ Hx,\ 0\ ]$ is selected. The electronic states in a magnetic field are characterized by three quantum numbers N, p_z and X, where N is the Landau quantum number, p_z the component of the momentum in the direction of magnetic field and X x-coordinate of the center of the cyclotron orbit. The unperturebed energy of the state (N, p_z, X) is given by

$$E^{(o)}(N, p_z, X) = (N + \frac{1}{2})\hbar\omega_c + \frac{\hbar^2 k_z^2}{2m} \ , \quad \omega_c = \frac{eH}{mc} \ . \tag{A.2}$$

The eigenfunction is represented by

$$\psi^o(N, p_z, X) = \frac{H_n(\frac{x - X}{\ell}) \exp(-\frac{(x - X)^2}{2\ell^2})}{\sqrt{2^N N!\ \sqrt{\pi}\ \ell}} \exp(ik_y y + ik_z z),$$

$$\ell = \sqrt{\hbar c / eH} \ , \tag{A.3}$$

where ℓ is the radius of the lowest Landau orbit, and $H_n(x)$ the Hermite polynominals.

The electron-phonon interaction Hamiltonian $\mathcal{H}_1$ will be discussed as follows. CdS is a crystal of the wurtzite structure and crystal class is $P6_3mc$. There are three independent piezoelectric constants[25] d_{33}, d_{31} and d_{15}. Namely, the nonzero piezoelectric components of d_{ijk} tensor are

$$d_{33} = d_{333} ,$$

$$d_{31} = d_{311} = d_{322} ,$$

$$d_{15} = d_{113} = d_{131} = d_{223} = d_{232} , \qquad (A.4)$$

where the axis 3 is the hexagonal axis and axis 1 and axis 2 are a pair of orthogonal axes lying in the plane perpendicular to the axis 3. In a piezoelectric material, an acoustic wave propargates being accompanied with polarization fields P_i which are given by

$$P_i = - d_{ijk} S_{jk} . \qquad (A.5)$$

Here i indicates direction of polarizations, and S_{jk} are strains caused by the elastic wave

For acoustic waves propagating to arbitrary directions, it is convenient to use the spherically averaged piezoelectric constants, according to the "isotropic interaction" model presented by Hutson[26]. The spherically averaged squares of electromechanical nondimensional coupling constants are

$$(K_\ell^2)_{av} = 4\pi \, (d_\ell^2)_{av} / \varepsilon c_\ell \quad \text{and} \quad (K_s^2)_{av} = 4\pi \, (d_s^2)_{av} / \varepsilon c_s , \qquad (A.6)$$

where d_ℓ and d_s are the piezoelectric constants for the longitudinal wave and the shear wave, respectively, ε is the dielectric constant, and c_ℓ, c_s are the elastic stiffness constants for the waves. The magnitude of the

coupling constants are given by Hutson[26] as

$$(K_\ell^2)_{av} = 0.0042 \quad \text{and} \quad (K_s^2)_{av} = 0.031 \ .$$

Therefore the shear modes give dominant contributions to the electro-mechanical coupling. The polarization field is simply rewritten as

$$P = \sqrt{(d_\ell^2)_{av}} \cdot S \quad . \tag{A.7}$$

As the strain caused by the acoustic phonon, it is given by the gradient of the displacement of lattice points (the dilation). The lattice displacement operator R is given by

$$R = \sqrt{\frac{\hbar}{V}} \sum_q e_q (2\rho\omega_q)^{-\frac{1}{2}} (b_q e^{iq\cdot r} + b_q^+ e^{-iq\cdot r}). \tag{A.8}$$

Here e_q is a unit vector in the direction of the polarization of the phonon, ρ the density, and $\hbar\omega_q$ the acoustic phonon energy. The dilation operator is given by

$$S = i \sqrt{\frac{\hbar}{V}} \sum_q (2\rho\omega_q)^{-\frac{1}{2}} q(b_q e^{iq\cdot r} - b_q^+ e^{-iq\cdot r}). \tag{A.9}$$

The electrostatic potential ϕ is expanded in the form

$$\phi (x) = \sum_q (\phi_a e^{iq\cdot r} + \phi_b e^{-iq\cdot r}) \ . \tag{A.10}$$

Hence,

$$E = - \mathit{grad}\ \phi = -i \sum_q (\phi_a e^{iq\cdot r} - \phi_b e^{-iq\cdot r}) \ . \tag{A.11}$$

Since, div D = 0; E = - $4\pi P$. We can rewite the interaction Hamiltonian $\mathcal{H}_1 = e\phi$ as follows:

$$\mathcal{H}_1 = \left(\frac{2\pi\alpha\hbar e^2 s}{\varepsilon V} \right)^{\frac{1}{2}} \sum_q \frac{1}{q\sqrt{q}} \left(b_q e^{iq\cdot r} + b_q^+ e^{-iq\cdot r} \right). \qquad (A.12)$$

where α is equal to $(K^2)_{av}$, and s (= ω_q / q) the velosity of the sound.

APPENDIX II

In the quantum limit ($\hbar\omega_c >> k_B T$), most of the electrons are in the ground state N = 0 of the Landau level. Therefore, the absorption of electromagnetic wave power is mostly due to the transitions from the states of N = 0 to those of N = 1 of the Landau levels. Therefore, the cyclotron frequency and the linewidth are determined by the energy and life time of the states N = 0 and N = 1. For instance, the shift of cyclotron resonant field is considered to originate from the difference of energy shifts between N = 0 and N = 1 levels. Schematic diagram of the Landau levels are shown in Fig. 22.

Unfortunately, the second-order perturbational calculation[10,13] cannot apply to know the energy shifts in a finite magnetic field, because the second order self-energy diverges for the interaction Hamiltonian $\mathcal{H}_1$. Thus it is necessary to treat the self-energy by a self-consistent method.

In the formalism of the second quantization, the Hamiltonian $\mathcal{H} = \mathcal{H}_0 + \mathcal{H}_1$ is rewritten as

$$\mathcal{H}_0 = \sum_\nu E^{(o)}(\nu)\, a_\nu^+ a_\nu + \sum_q \hbar sq\, b_q^+ b_q \quad ,$$

$$\mathcal{H}_1 = \left(\frac{4\pi\alpha\hbar^2 e^2 s^2}{\varepsilon V} \right)^{\frac{1}{2}} \sum_q \sum_{\nu,\nu'} \left(\nu | e^{iq\cdot r} | \nu' \right) a_\nu^+ a_{\nu'} \times (2\hbar sq)^{-\frac{1}{2}} (b_q + b_{-q}^+) \quad , \qquad (A.13)$$

where ν represents a set of quantum numbers (N, p_z, X) and a_ν^+ and a_ν are the creation and annihilation operators of an electron in the state ν.

The one-electron Green's function is defined by

$$G(\nu, t-t') \equiv -i \langle T\, a_\nu(t)\, a_\nu^+(t') \rangle \quad , \qquad (A.14)$$

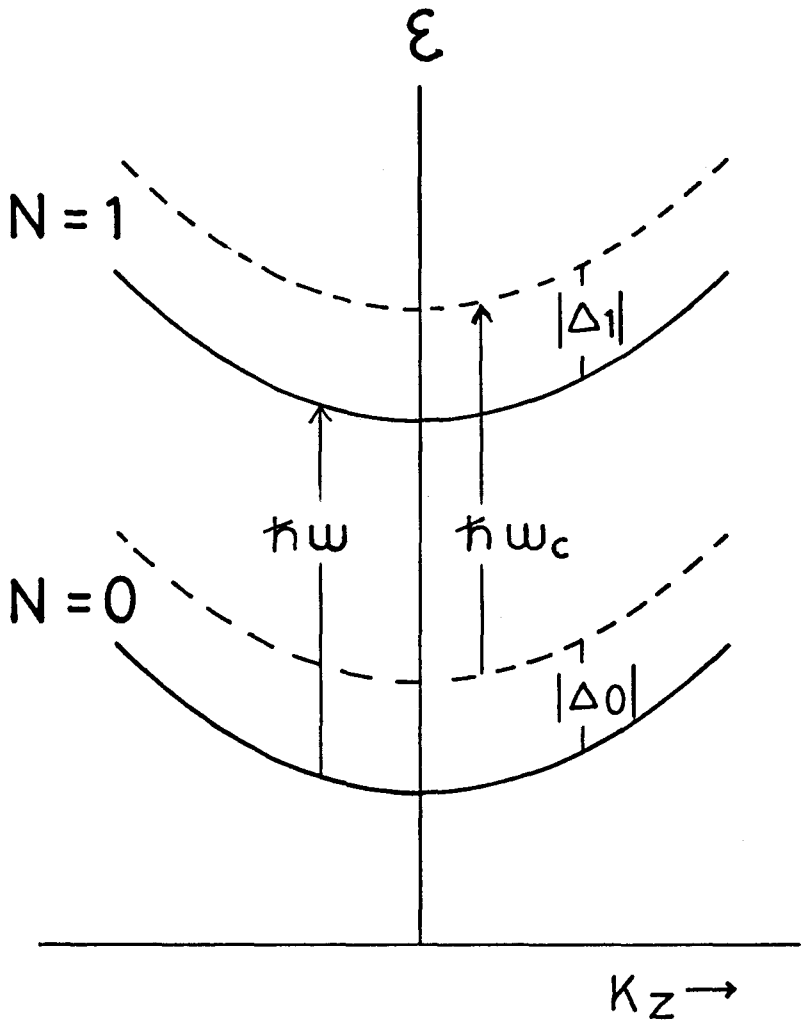

Fig. 22. Schematic diagram of energy shifts of Landau levels N = 0 and N = 1 due to electron-phonon interaction. ---- unperturbed levels.

and the phonon Green's function

$$D(q, t-t') \equiv - \frac{1}{2\hbar sq} < T\,[b_q(t) + b^+_{-q}(t)][b^+_q(t') + b_{-q}(t')] >. \qquad (A.15)$$

Here t and t' are the "imaginary time" variables and T is the Wick's time-ordering operator. <Q> indicates the average over a grand canonical ensemble:

$$<Q> \equiv \frac{Tr\{ \exp[-\beta(\mathcal{H} - \mu N)]Q \}}{Tr\{ \exp[-\beta(\mathcal{H} - \mu N)]\}} ,$$

$$N = \sum_\nu a^+_\nu a_\nu \quad , \quad \beta = 1 / k_B T . \qquad (A.16)$$

Here μ is the chemical potential of the electron, N the operator of the total number of particles and a(t) and b(t) are the Heisenberg representation of the operators a and b.

For the Green's functions there are important relations;

$$G(q\ ,\ -i\beta\ ) = -\ G(q\ ,\ 0)e^{-\beta\mu} , \qquad (A.17)$$

$$D(q\ ,\ -i\beta\ ) = D(q\ ,\ 0\ ) . \qquad (A.18)$$

They can be expanded into Fourier series:

$$G(\nu, t) = \frac{i}{\beta} \sum_n e^{-i\zeta_n t} G(\nu, \zeta_n), \quad \zeta_n = \mu + i\,\frac{(2n+1)\pi}{\beta} , \qquad (A.19)$$

$$D(q, t) = \frac{i}{\beta} \sum_j e^{-i\omega_j t} G(q, \omega_j), \quad \omega_j = i\,\frac{2j\pi}{\beta} . \qquad (A.20)$$

The Dyson equation is given by

$$G(\nu, \zeta_n) = \frac{1}{G^{(o)}(\nu, \zeta_n)^{-1} - \Sigma(\nu, \zeta_n)} = \frac{1}{\zeta_n - E^{(o)}(\nu) - \Sigma(\nu, \zeta_n)} , \tag{A.21}$$

$$\Sigma(\nu, \zeta_n) = - \frac{4\pi\alpha\hbar^2 e^2 s^2}{\beta\varepsilon V} \sum_j \sum_q \sum_{\nu'} G(\nu', \zeta_n - \omega_j)$$

$$\times D(q, \omega_j) |(\nu|e^{iq\cdot r}|\nu')|^2 \Gamma_q(\nu: \nu'; \zeta_n, \omega_j), \tag{A.22}$$

where Γ_q is the vertex function, which is normalized.

We make an approximation for the phonon Green's function as follows;

(1) The self-energy of phonons is negligible when the number of the electron is small.

(2) The thermal energy is much larger than the energy of phonons ($k_B T >> \hbar sq$).

(3) Γ_q can be approximated by its lowest value ($\Gamma_q = 1$). Then we obtain a simplified phonon Green's function:

$$D(q, \omega_j) \approx D^{(o)}(q, \omega_j) = \frac{1}{2\hbar sq} \left[\frac{1}{\omega_j - (\hbar sq)} - \frac{1}{\omega_j + (\hbar sq)}\right]$$

$$= \frac{1}{\omega_j^2 - (\hbar sq)^2} \approx - \delta_{j,0} \frac{1}{(\hbar sq)^2} . \tag{A.23}$$

In the Eq. (A.21), the variables ζ_n is analytically continued to the real axis. The self-energy function is rewritten as

$$\Sigma(\nu: E \pm i\delta) = \frac{4\pi\alpha e^2}{\beta\varepsilon V} \sum_q \sum_{\nu'} \frac{1}{q^2} \frac{|(\nu'|e^{iq\cdot r}|\nu)|^2}{E \pm i\delta - E^{(o)}(\nu') - \sum(\nu'; E \pm i\delta)} , \tag{A.24}$$

$$\Sigma = \mathrm{Re}\,\Sigma + i\,\mathrm{Im}\,\Sigma \equiv \Delta + i\Gamma . \tag{A.25}$$

Replacing the real part of the denominator of electron Green's function by zero, we obtain the quasiparticle energy of the state $(N, p_z, X) \equiv \nu$ as,

$$E = E^{(o)}(\nu) + \Delta(\nu; E). \tag{A.26}$$

On the other hand, the life-time can be determined from the imaginal part of the denominator, i.e., $\Gamma(\nu; E)$.

Equations (A.24) and (A.26) constitute a complicated set of simultaneous integral equations. In order to solve these equations the following approximation is adopted:

(1) Neglecting the dependence of $\Sigma(N, p_z, X; E)$ on p_z, we replace Σ by its value at $p_z = 0$. Moreover, considering Σ being independent of X, we may write this quantity as $\Sigma_N(E)$.

(2) The self-energy function Σ in the denominator in Eq. (A.24) is considered to be necessary to take into account only when the denominator would become zero without Σ. In other words, we retain the self-energy function Σ in the denominator only if $N' \leq N$.

In order to calculate the self energy function Σ in the quantum limit ($\hbar\omega_c >> k_B T$), we may take into account only the state $N = 0$ and $N = 1$ for the state $|\ \nu)$ in the numerator of Eq. (A.24). The matrix elements are represented by

$$|(N', p_z', X'|e^{iq\cdot r}|\ 0, p_z, X)|^2$$

$$= \delta_{p_z', p_z+\hbar q_z} \cdot \delta_{x', x-\ell^2 q_y} \frac{1}{N'!} \left(\frac{\ell^2 q_\perp^2}{2} \right)^{N'} \exp\left(- \frac{\ell^2 q_\perp^2}{2} \right), \tag{A.27}$$

$$|(N', p_z', X'|e^{iq\cdot r}|\ 1, p_z, X)|^2$$

$$= \delta_{p_z', p_z+\hbar q_z} \cdot \delta_{x', x-\ell^2 q_y} \frac{1}{N'!} \left(\frac{\ell^2 q_\perp^2}{2} \right)^{N'-1} \left(N' - \frac{\ell^2 q_\perp^2}{2}\right)^2 \exp\left(- \frac{\ell^2 q_\perp^2}{2} \right), \tag{A.28}$$

where $q_\perp^2 = q_x^2 + q_y^2$, $q^2 = q_\perp^2 + q_z^2$.

The energy of the N-th Landau level is given by

$$E_N = E^{(o)}(N,\ p_z = 0) + \Delta_N(E_N), \qquad (N = 0,\ 1,\ 2,\ \cdots\cdots\ ). \tag{A.29}$$

For simplifying the expressions, we introduce dimensionless wave numbers and the self-energy,

$$u = \sqrt{\frac{\ell^2 q_\perp^2}{2}} \ , \quad \xi = \sqrt{\frac{\ell^2 q_z^2}{2}} \quad \text{and}$$

$$d_{N'N} + i g_{N'N} = \frac{\Delta_{N'}(E_N)}{\hbar\omega_c} + i\,\frac{\Gamma_{N'}(E_N)}{\hbar\omega_c} = \frac{\Sigma_{N'}(E_N)}{\hbar\omega_c} \ . \tag{A.30}$$

We obtain for the self-energy function for N = 0:

$$d_0 + i\, g_0 = \frac{\lambda}{\pi} \sum_{N'} \frac{1}{N'!} \int_0^\infty du \int_{-\infty}^{\infty} d\xi\, \frac{u}{(u^2 + \xi^2)}$$

$$\times \frac{u^{2N'} e^{-u^2}}{[E^{(o)}_{(0,p_z=0)} - E^{(o)}_{(N',p_z')}]/\hbar\omega_c + d_0 - (d_{N'0} + i q_{N'0})} \ ,$$

$$\lambda = \sqrt{2}\ \alpha\ (\ell/a_B)(K_B T/\hbar\omega_c), \tag{A.31}$$

where d_N and g_N indicate d_{NN} and g_{NN}, respectively, and $a_B = (\hbar^2\epsilon/me^2)$ is the effective Bohr radius. In the above approximations, Eq. (A.31) is reduced to

$$d_0 + i\, g_0 = -\lambda \left\{ \frac{1}{\pi} \int_0^\infty du \int_0^\infty d\xi\ \frac{u\, e^{-u^2}}{(u^2 + \xi^2)(\xi^2 + i\, g_0)} + S_1 \right\}, \tag{A.32}$$

where

$$S_1 = \frac{1}{\pi} \sum_{N'=1}^{\infty} \frac{1}{N'!} \int_0^{\infty} du \int_{-\infty}^{\infty} d\xi \; \frac{u\, e^{-u^2} u^{2N'}}{(u^2 + \xi^2)(\xi^2 + N')} \,. \tag{A.33}$$

The summation S_1 can be translated into integral using the transformation: $1/x = \int_0^{\infty} dt \exp(-xt)$, $(x > 0)$, then S_1 has the form

$$S_1 = \frac{1}{\pi} \int_0^{\infty} dk \int_{-1}^{1} d\mu \int_0^{\infty} dt \exp[-k^2(1-\mu^2+\mu^2 t)]\{ \exp[k^2(1-\mu^2)e^{-t}] - 1 \} , \tag{A.34}$$

where $u = k \sin\theta$ and $\xi = k \cos\theta = k\mu$. The integral of the first term in the bracket of Eq. (A.32) can be slightly simplified, and Eq. (A.32) for the self-energy of the lowest Landau level is reduced to

$$d_0 + i\, g_0 = - \lambda \{ \int_0^{\infty} du \frac{e^{-u^2}}{\sqrt{i g_0}\, [\, \sqrt{i g_0} + u]} + S_1 \} \,. \tag{A.35}$$

Besides, the self-energy for $N = 1$ is given by

$$d_1 + i\, g_1 = \frac{\lambda}{\pi} \sum_{N'} \frac{1}{N'!} \int_0^{\infty} du \int_{-\infty}^{\infty} d\xi \; \frac{u}{(u^2 + \xi^2)}$$

$$\times \frac{U^{2(N'-\xi)} (N' - u^2)^2 e^{-u^2}}{[E^{(0)}(1,\, p_z=0) - E^{(0)}(N', p_z')]/\hbar\omega_c + d_1 - (d_{N'1} + i\, g_{N'1})} \,. \tag{A.36}$$

Using the same method as the above mentioned, we abbreviate Eq. (A.36) as

$$d_1 + i\, g_1 \cong - \lambda \{ \int_0^{\infty} du \frac{u^2 e^{-u^2}}{\sqrt{i g_{01} + d_{01} - d_1 - 1}\, (\sqrt{i g_{01} + d_{01} - d_1 - 1} + u)}$$

$$+ \int_0^{\infty} du \frac{(1 - u^2)^2 e^{-u^2}}{\sqrt{i g_1}\, (\sqrt{i g_1} + u)} + S_2 \} , \tag{A.37}$$

where

$$S_2 = S_1 + \int_0^\infty dk \int_{-1}^{1} d\mu \int_0^\infty dt\ k^2(1-\mu^2)\exp[-(k^2-k^2\mu^2+k^2\mu^2 t)]$$

$$\times \{ (e^t+e^{-t}+2)\exp[k^2(1-\mu^2)e^{-t}] - (e^t-2)-k^2(1-\mu^2) \}. \qquad (A.38)$$

In the calculation of Eq. (A.37), if we assume for simplification that $d_{01} = d_1$ and $g_{01} = g_1$, the following expression is derived,

$$d_1 + i\, g_1 = -\lambda \{ \int_0^\infty du \frac{u^2 e^{-u^2}}{\sqrt{ig_1 - 1}\ (\sqrt{ig_1 - 1} + u)}$$

$$+ \int_0^\infty du\ \frac{(1-u^2)^2 e^{-u^2}}{\sqrt{ig_1}\ (\sqrt{ig_1} + u)} + S_2 \}. \qquad (A.39)$$

Thus, by numerical calculation, we can obtain d_0, d_1, g_0 and g_1 as a function of λ.

(1) Half line width

The line width of the cyclotron resonance in the quantum limit, ΔH, is expressed by the imaginary term of the self-energy as $\Gamma_0 = g_0 \hbar\omega_c$ and $p_1 = g_1 \hbar\omega_c$. Carrying out the numerical calculation of g_0 and g_1, we can obtain the following relation in an approximation:

$$g_0 \simeq g_1 \sim 0.76\ \sqrt{\lambda}\ \propto T^{\frac{1}{2}} H^{-\frac{3}{4}}, \qquad (A.40)$$

where the coupling constant λ was previously defined as

$$\lambda = \sqrt{2}\ \alpha\ (\ell / a_B)\ (k_B T / \hbar\omega_c).$$

Hence the half line width of the cyclotron resonance is given by

$$\frac{\Delta H}{H^*} \sim \frac{\Gamma_0 + \Gamma_1}{\hbar\omega_c} \sim 1.5\sqrt{\lambda} \qquad (A.41)$$

(2) The cyclotron mass shift

The shift of the energy separation between the 0-th and 1-st Landau levels is given by

$$\Delta_1(E_1) - \Delta_0(E_0) = (d_1 - d_0)\hbar\omega_c \sim 0.18\,\lambda^{2/3}\hbar\omega_c \,. \qquad (A.42)$$

Taking into account that ω_c is the unperturbed cyclotron frequency, the mass shift is estimated to be

$$\frac{m}{m^*} - 1 \sim 0.18\,\lambda^{2/3} \,. \qquad (A.43)$$

Here m^* is the mass which should be observed in the cyclotron resonance experiment.

REFERENCES

1) H. J. G. Meijer and D. Polder: Physica 19 (1953) 225.

2) W. W. Piper and R. E. Halsted: Proceeding of the International Conference on Semiconductor Physics. (1960) 1046.

3) H. Fujita, K. Kobayashi, T. Kawai and K. Shiga: J. Phys. Soc. Japan 20 (1965) 109.

4) K. Kobayashi and F. C. Brown: Phys. Rev. 113 (1959) 507.

5) J. J. Hopfield and P. G. Thomas: Phys. Rev. 122 (1961) 35.

6) W. W. Piper and D. T. F. Marple: J. appl. Phys. 32 (1961) 2237.

7) K. Sawamoto: J. Phys. Soc. Japan 19 (1964) 318.

8) W. S. Baer and R. N. Dexter: Phys. Rev. 135 (1964) A1388.

9) G. D. Mahan and J. J. Hopfield: Phys. Rev. Letters 12 (1964) 241.

10) D. M. Larsen: Phys. Rev. 142 (1966) 428.

11) M. Saitoh and A. Kawabata: J. Phys. Soc. Japan 23 (1967) 1006.

12) R. Kubo: J. Phys. Soc. Japan 12 (1957) 570.

13) S. J. Miyake: Phys. Rev. 170 (1968) 726.

14) K. Button, B. Lax and D. R. Cohn: Phys. Rev. Letters 24 (1970) 375.

15) T. L. Cronburg and B. Lax: Phys. Letters 37A (1971) 135.

16) K. Nagasaka, G. Kido and S. Narita: J. Phys. Soc. Japan 28 (1970) 1376.

17) S. Narita, K. Nagasaka and G. Kido: Proceeding of the International Conference on Semiconductor Physics. (1970) 158.

18) G. Kido, K. Nagasaka and S. Narita: Japanese J. appl. Phys. 11 (1972) 237.

19) Products of Asahi-Garasu, Inc.

20) M. Cardona: Solid State Physics Suppl. 11, Modulation Spectroscopy ed. F. Seitz, D. Turnbull and H. Ehrenreich (Academic Press, New York, London, 1969) p. 101.

21) M. Porsch: Phys. Letters 30A (1969) 416.

22) K. Okamoto: J. Phus. Soc. Japan 32 (1972) 46.

23) C. A. Arguello, D. L. Rousseau and S. P. S. Porto: Phys. Rev. 181 (1969) 1351.

24) F. G. Bass and I. B. Levinson: Soviet Phys. JETP 22 (1966) 635.

25) J. E. Nye: Physical Properties of Crystals (Oxford, 1957) p. 300.

26) A. R. Hutson: J. appl. Phys. 32 (1961) 2287.